Comptes Rendus

Physique

Abhinav Bhardwaj, Dheeraj Pratap, Mitchell Semple, Ashwin K. Iyer,
Arun M. Jayannavar and S. Anantha Ramakrishna

Properties of waveguides filled with anisotropic metamaterials

Metamaterials 2 / *Métamatériaux 2*

Properties of waveguides filled with anisotropic metamaterials

Propriétés de guides d'ondes constitués d'un métamatériau anisotrope

Abhinav Bhardwaj [a]**, Dheeraj Pratap** [b]**, Mitchell Semple** [c]**, Ashwin K. Iyer** [c]**,
Arun M. Jayannavar** [d] **and S. Anantha Ramakrishna**[*, e, f]

[a] Department of Electrical Engineering, Indian Institute of Technology Kanpur, Kanpur, 208016, India

[b] Biomedical Instrumentation Division, CSIR — Central Scientific Instruments Organisation, Sector-30C, Chandigarh 160030, India

[c] Department of Electrical and Computer Engineering, University of Alberta Edmonton, Alberta T6G2V4, Canada

[d] Institute of Physics, Sachivalaya marg, Bhubaneswar, 751005, India

[e] CSIR — Central Scientific Instruments Organisation, Sector-30C, Chandigarh 160030, India

[f] Department of Physics, Indian Institute of Technology Kanpur, Kanpur, 208016, India

E-mails: Abhinavb@iitk.ac.in (A. Bhardwaj), dheeraj.pratap@csio.res.in (D. Pratap), msemple@ualberta.ca (M. Semple), iyer@ece.ualberta.ca (A. K. Iyer), jayan@iopb.res.in (A. M. Jayannavar), sar@iitk.ac.in (S. A. Ramakrishna)

Abstract. Metamaterials are artificially structured composite materials that show unusual properties not usually available in natural materials. In general, metamaterial structures and properties are anisotropic. A waveguide filled with an anisotropic metamaterial shows unique properties not achievable in conventional waveguides, such as propagation of backward waves and modes below the cut-off frequencies of the conventional fundamental mode, zero group velocity etc. The waveguide filler material can be anisotropic with the tensorial permittivity and permeability components having positive or negative values, and combinations thereof, giving rise to a rich variety of phenomena. Further, modes in a cylindrical waveguide filled with a hyperbolic metamaterial are described by unusual Bessel modes of complex orders. In many situations, the wave propagating region is isotropic, and it is enclosed by anisotropic metamaterials with different thicknesses and contrarily the propagating region is might be anisotropic that is enclosed by isotropic in some other situations. Various metamaterial waveguide geometries like a pair of parallel plates, waveguides with rectangular or cylindrical cross-section filled with anisotropic metamaterials as well as hollow-core waveguides with metamaterial claddings or linings have been demonstrated experimentally. The anisotropy can

* Corresponding author.

be uniaxial or biaxial depending on the orientation of structure. Here we review the advances in the theory and applications of waveguides filled with subwavelength structured metamaterials with anisotropic or even hyperbolic properties across the electromagnetic spectrum. By examining the field behaviour in such waveguides, connection is made to the extraordinary transmission of light through arrays of subwavelength sized apertures in a metallic screen. Potential applications range from enhanced MRI imaging and electromagnetic shielding at radio frequencies to intriguing imaging applications and efficient coupling of the emitted radiation from small sources into waveguides at optical frequencies.

Résumé. Les métamatériaux sont des matériaux composites structurés de manière artificielle qui possèdent des propriétés que l'on ne trouve pas à l'état naturel. En général, les propriétés structurelles des métamatériaux sont anisotropes. Un guide d'ondes constitué d'un métamatériau possède des propriétés uniques inatteignables dans des guides d'ondes conventionnels, telles que la propagation d'onde rétrogrades et des modes sous les fréquences de coupure du mode fondamental d'un guide d'ondes conventionnel, une vitesse de groupe nulle etc. Le matériau constituant le guide d'ondes peut être anisotrope avec les éléments (ou des combinaisons d'éléments) des tenseurs de permittivité et perméabilité qui prennent des valeurs positives ou négatives, ce qui donne lieu à une riche variété de phénomènes. Par ailleurs, les modes d'un guide d'ondes cylindrique constitué d'un métamatériau hyperbolique sont décrits par des fonctions de Bessel inhabituelles présentant des ordres complexes. Dans de nombreuses situations, la région siège de la propagation d'ondes est isotrope, et est entourée de métamatériaux anisotropes avec différentes épaisseurs et inversement. Diverses géométries de guides d'ondes en métamatériaux tels que des paires de plaques parallèles, des guides rectangulaires et cylindriques constitués de milieux anisotropes, ainsi que des guides d'ondes à cœur creux avec une gaine en métamatériaux ou des *linings* ont été démontrés expérimentalement. L'anisotropie peut être uniaxe ou biaxe en fonction de l'orientation de la structure. Nous faisons un état de l'art sur les avancées dans la théorie et les applications des guides d'ondes constitués de métamatériaux avec une structuration sub-longueur d'onde dont les propriétés sont anisotropes ou même hyperboliques sur le spectre électromagnétique. En examinant le comportement du champ dans ce type de guides d'ondes, un lien est établi avec la théorie de la transmission extraordinaire de la lumière à travers des réseaux de trous sub-longueur d'onde dans un écran métallique. Les applications potentielles vont de l'imagerie médicale à résonance magnétique améliorée au bouclier électromagnétique aux fréquences radio en passant par des applications étonnantes en imagerie et au couplage efficace des émissions de petites sources avec des guides d'ondes aux fréquences optiques.

1. Introduction

Ever since Sir John Pendry gave recipes [1, 2] to generate composite media with negative effective parameters like dielectric permittivity and magnetic permeability at any given frequency, the electromagnetics and optics of structured composite media have been among the most popular topics in the past twenty years. These composite metal-dielectric materials, commonly called metamaterials, typically had small sub-wavelength sized units cells, and the composites could be described by effective medium theories. Veselago first proposed a negative refractive index medium as a material with simultaneously negative permittivity and permeability and treated it as an isotropic medium [3]. During the first decades of this century, many of the fundamental aspects of such media were understood and novel phenomena such as negative refraction [4], image resolution without any limit [5] and several novel effects were experimentally realised in structured composite media. Use of the most modern techniques of micro and nano fabrication enabled the demonstration of these effects from microwave frequencies up to optical frequencies [6,7]. While much of the theory initially dealt with isotropic metamaterials (composite structure), almost all the fabricated metamaterials were anisotropic [8]. This was partially caused by

the severe difficulty of assembling isotropic metamaterials, particularly at high frequencies, when the wavelength of radiation and the corresponding structural sizes become micrometric or even nanometrically small in size. Further, the requirement of an isotropic medium was not necessary for realizing many effects. It was further noted that anisotropic metamaterials could easily have one or two diagonal components of the permittivity or the permeability tensor becoming negative, while the others were positive. These tensors with indefinite signs resulted in the dispersion equations changing their form qualitatively from elliptic to hyperbolic equations [9, 10]. This was a new effect in optics and electromagnetism, where such dispersions lead to qualitatively new phenomena such as the hyperlens [10], and such media had infinities in the local density of states [11]. Thus, understanding the new possible effects possible in anisotropic media and hyperbolic media became imperative as metamaterials that had such properties became possible to fabricate.

Propagation of electromagnetic waves in a waveguide is well understood with the optical fiber becoming probably the most commonly used example of a waveguide. With the advent of metamaterials with exotic properties, researchers naturally investigated the properties of waveguides filled with metamaterials, particularly negative refractive index materials [12–16]. Waveguides filled with metamaterials could support propagation of electromagnetic modes with strange properties such as zero or negative group velocity, modes below the cutoff frequencies of the fundamental modes, and the absence of a fundamental mode [16–18]. These investigations naturally turned to the study of waveguides filled with anisotropic/hyperbolic metamaterials. Some interesting effects such as the propagation of modes well below the conventional cutoff were discovered, which were attractive for possibilities of miniaturization of radio frequency (RF) waveguide components, particularly in the context of magnetic resonance imaging (MRI) [17,19].

At high frequencies such as optical and infrared frequencies, while there were a few theoretical studies [14, 16, 20], one was faced with the ostensibly impossible task of assembling millions or billions of micro/nano structures into microscopic volumes in an ordered fashion. Following the conventional techniques of drawing photonic crystal fibers [21], researchers attempted to draw fibers with embedded structural units such as metallic split ring resonators [22] or coaxial thin metallic wires [23, 24] for operation at THz frequencies. The first successful nanostructured metamaterial fiber for optical frequencies was realized by Pratap *et al.* [13], where they anodized an aluminum wire to successfully form a microtube of nanoporous alumina with radially emanating pores that could be filled electrolytically with plasmonic metals. This made waveguides filled with cylindrically symmetric anisotropic media realistically possible. Such waveguides were shown to support novel propagating modes described by unusual Bessel functions with complex orders [13]. Abhinav *et al.* have shown that light emanating from subwavelength-sized sources can be efficiently coupled into such waveguides [16]. Several novel effects appear possible, given the large variety of free parameters (components of the ε and μ tensor) that can be chosen here. Waveguides filled or lined with anisotropic metamaterials potentially have great utility in the context of guiding radio-waves in MRI applications where the anisotropic metamaterials play a major role in increasing throughput or coupling in the subwavelength sized waveguide. It was shown that anisotropy was a pre-requisite for negative refraction and focusing of guided surface plasmon waves on the interfaces of anisotropic negative-positive permittivity metamaterials [25].

We offer here a review of the advances in waveguides filled with anisotropic metamaterials. Our purpose is to introduce a young researcher to the new developments while logically developing the ideas behind the exciting advances. Starting with a quick introduction to the ideas of metamaterials and effective medium properties, we will introduce recent work carried out on metamaterial filled waveguides, particularly waveguides filled with negative refractive index materials and anisotropic metamaterials. We will then move on to describe the guided modes in these systems: first in rectangular and parallel plate waveguide geometries followed by cylindrical

waveguides with cylindrically symmetry anisotropies. The behaviour of the propagating modes in various manifestations of these waveguides are discussed with a view to project out various kinds of applications for these waveguides at both optical and radio/microwave frequencies. A mapping of the waveguide phenomena to apertures in metallic screens, and subsequently periodic arrays of apertures that usually comprise metasurfaces, will also be described. Here, metamaterial liners have found application in the realization of compact aperture arrays demonstrating extraordinary free-space wave-manipulation properties that may be engineered to enable a multitude of functionalities. As such, these metamaterial-lined aperture arrays may be referred to as resonant metasurfaces. It is critical to appreciate that the description here, while being rigorous, cannot be comprehensive given the wide variety of phenomena possible. We will conclude with an outlook for future work in these areas.

2. General concept of metamaterial waveguides

An electrically neutral plasma has a dielectric permittivity given by

$$\varepsilon(\omega) = 1 - \frac{\omega_p^2}{\omega(\omega + \mathrm{i}\gamma)} \tag{1}$$

where $\omega_p^2 = ne^2/m_e\varepsilon_0$ is the plasma frequency determined by n, the number density of free charge carriers, e, is the charge, m_e, the mass of the charge carriers, and ε_0 is the vacuum permittivity. The γ is a phenomenological parameter that determines dissipation of the electromagnetic wave. There can be both positive and negative charges with different masses in a plasma, resulting in multiple plasma frequencies corresponding to each species.

2.1. *Metamaterials: thin wire medium and split ring resonator*

All good conductors are free electron plasmas that have $\varepsilon < 0$ for frequencies lower than the plasma frequency that typically lies at ultra-violet frequencies for metals like gold, silver, aluminium and copper. But, the large magnitude of $\mathrm{Re}(\varepsilon)$ parameters at the frequencies much lower than the plasma frequency does not allow plasmonic effects and applications to be easily realized in conductors [26]. Pendry *et al.* proposed that arrays of thin metallic wires as shown in Figure 1(a) behave as plasmas with much lowered plasma frequencies [27]. The radius of the wires can be sub-millimeter, micrometer and nanometer for radio, infrared and optical frequencies respectively [24]. The wire medium behaves as an effective medium if the radius of metal wire (r) is much smaller than the separation between wires (p) and both are much smaller than the wavelength the radiation (λ) ($r \ll p \ll \lambda$). Such as medium was shown to have a plasma-like dielectric permittivity with $\omega_p^2 = 2\pi c^2/p^2 \ln(p/r)$ that is seen to be determined merely by the geometric parameters of the structure. The large inductance of thin wires plays an important role in reducing the plasma frequency. The relative permittivity of a wire medium oriented only in one direction as shown in Figure 1(a) [27] has an uniaxial diagonal tensor $(\epsilon_t, \epsilon_t, \epsilon_z)$ with $\varepsilon_z < 0$, where the axis of the wires is assumed parallel to the z-axis. A three-dimensional lattice of thin wires could behave as an isotropic low-frequency plasma.

Pendry *et al.* also first demonstrated the ability to obtain dynamic magnetic polarizability in metallic composites consisting of coupled split ring resonators (SRR), shown schematically in Figure 1(b) [2]. When the incident magnetic field vector is along the axis of the rings (SRR), an electromotive force is induced around the rings. The currents in the two rings get coupled through a distributed capacitance formed between the rings (due to the gap). This results in the structure acting as a resonant L-C circuit, driven by the magnetic field of the incident electromagnetic wave. The SRR medium forms a uniaxial magnetic medium if the axis of the ring
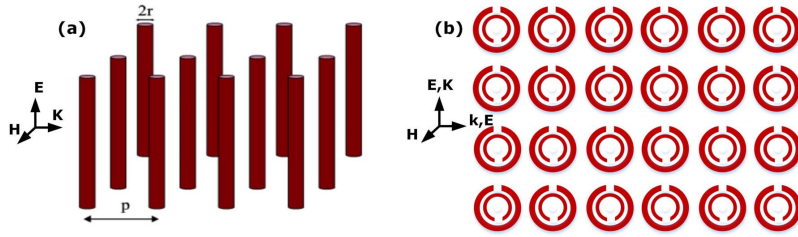
Figure 1. (a) Thin wire medium (b) 2D Image of a series of split ring resonators.

and the magnetic fields only along one direction. Smith *et al.* experimentally obtained negative refractive index media by combining thin wire and SRR structures with overlapping frequency ranges of negative permittivity and permeability [4].

2.2. *Effective medium theory*

In metamaterials, the composite (host and inclusion) materials are typically smaller than the wavelength of radiation, but much larger than the molecules or atoms. The periodic structure (unit cells) of these materials or their structural constituents can not be resolved by the wave and the material can be characterized by effective medium parameters such as relative permittivity and permeability. The effective medium parameters are obtained by appropriate averages of fields over the unit cell within the metamaterial [2].

The Maxwell–Garnett homogenization describes composites with small volume fraction of inclusion materials by incorporating the distortions due to the dipole fields of the inclusions on an average. Let us assume that a spherical particle having relative permittivity ε_i is embedded in a bulk host material of relative permittivity ε_h. The effective permittivity of this composite medium is

$$\epsilon_{\text{eff}} = \epsilon_h \frac{\epsilon_i (1 + 2f) + 2\epsilon_h (1 - f)}{\epsilon_i (1 - f) + \epsilon_h (2 + f)}, \tag{2}$$

where f is the volume filling fraction of the inclusions [26]. This method is valid for a fill-fraction up to about 0.3. An alternate process called the Bruggeman homogenization treats the inclusions and host constituents on equal footing and is valid for higher fill-fractions of inclusions also [28, 29]. The effective medium parameters can also be obtained from the modeling of the re-emission (reflection and transmittance) of light incident on the medium [8], a process that is often called the *Parameter retrieval procedure*.

Guenneau *et al.* homogenized three dimensional finite photonic crystals and waveguides filled with magneto-dielectric inclusions using a two-scale convergence to realize anisotropic effective media [30]. The problems of obtaining homogenized medium properties from emergent quantities using parameter retrieval methods for anisotropic media with aribitrarily oriented axes [31] and even bianisotropic metamaterials [32–35] have been addressed. Aspects of causality in such retrieval methods have been discussed [36, 37]. Usually, magneto-dielectric coupling or bianisotropy is not very strong in most metamaterials, although it is present in many, and most of the models do not explicitly include bianisotropy [38]. In our cases, most of the structures do not have much bianisotropy and it is not discussed here.

2.3. *Anisotropic, hyperbolic, zero permittivity and permeability*

Metamaterials, like thin wire array media, and SRR media can be modeled as anisotropic media characterized by permittivity and permeability tensors

$$
\overline{\overline{\varepsilon}} = \begin{pmatrix} \epsilon_x & 0 & 0 \\ 0 & \epsilon_y & 0 \\ 0 & 0 & \epsilon_z \end{pmatrix}, \quad \overline{\overline{\mu}} = \begin{pmatrix} \mu_x & 0 & 0 \\ 0 & \mu_y & 0 \\ 0 & 0 & \mu_z \end{pmatrix}, \tag{3}
$$

in a reference frame with appropriately oriented axes. As an example, consider an array of nanometrically thin long metallic wires, all oriented along the z-axis, at optical frequencies when the fields will completely penetrate across the nanometric wire. Such a system is realized by electrolytically deposited silver or copper wires in a nanoporous alumina template with oriented long nanoholes [39]. An electromagnetic wave polarized along the z-axis would experience an effective permittivity of $\varepsilon_z(\omega) = f\varepsilon_m(\omega) + (1-f)\varepsilon_h(\omega)$, where $\varepsilon_m(\omega)$ is the permittivity of the metal, $\varepsilon_h(\omega)$ is the host (alumina) permittivity, and f is the fill fraction of the metal. For the orthogonal polarization perpendicular to the axis of the cylindrical wires, one may derive an expression for the effective permittivity (similar to (2) for spherical inclusions). The material properties are different for different directions of the polarization of the wave. The dispersion relation of a plane wave propagating in an anisotropic metamaterial with the electric field polarized along the z-axis can be written as

$$
\frac{k_y^2}{\epsilon_x} + \frac{k_x^2}{\epsilon_y} = \frac{\mu_z \omega^2}{c^2}, \tag{4}
$$

where ω, k_x, k_y, c are the angular frequency of the wave, x component of the wave vector, y component of the wave vector, and speed of light in free space respectively. The material tensor components $(\varepsilon_x, \varepsilon_y, \mu_z)$ are experienced by the transverse magnetic polarized plane wave. The dispersion relation is an elliptical curve in the iso-frequency plane for metamaterials with all positive index diagonal tensors of relative permittivity and permeability. Waveguides filled with anisotropic materials have many unusual properties due to this elliptical dispersion, as demonstrated by Dheeraj *et al.* [13]. The diagonal components of the permittivity and permeability tensors may not have the same sign, in which case the dispersion relation (4) becomes a hyperbolic curve in the iso-frequency plane [9]. Such media are said to display "hyperbolic" (indefinite) dispersion and have capability to strongly enhance spontaneous emission due to the diverging density of states [11, 40], and can show negative refraction and enhanced perfect lensing effects [16, 41]. Multilayered stacks of metal-dielectric thin films, multilayer fishnet structures and thin wire media are examples of hyperbolic media [41, 42]. With an anisotropic and hyperbolic cladding, Shaghik *et al.* analyzed that the hollow circular waveguides can guide modes with extremely subwavelength sized core diameters [14]. A circular waveguide filled with a hyperbolic metamaterial can support modes having upper but no lower cutoff frequency and enhance the power coupled from subwavelength sized sources [16].

Metamaterials exhibiting near-zero permittivities, known as epsilon-near-zero or ENZ metamaterials, have received a great deal of attention for their utility in the creation of compact resonators. One application is the homogeneous ENZ-filled metallic waveguide demonstrated by Alù and Engheta, which permits the transmission of power for arbitrarily small cross sections and waveguide geometries by way of a tunneling-like mechanism [15]. Transmission through such electrically small cross-sections is tantamount to an extreme reduction of the cutoff frequency of the fundamental waveguide mode. A generalization of this idea was put forth by Pollock and Iyer, who examined partially, or inhomogeneously, filled metallic waveguides—in particular, perfect electric conductor (PEC) circular waveguides lined using a thin coating of ENZ

metamaterial [17]. It was determined that, for propagation through circular waveguides of arbitrarily small cross-section, the ENZ property was necessary but not sufficient: whereas a positive and near-zero permittivity drives the waveguide further into cutoff, a negative and near-zero permittivity is required to operate the waveguide well below cutoff. This is achieved through the introduction of a new low-frequency and backward-wave passband. This property was therefore termed epsilon-negative and near-zero, or ENNZ. The notion of thin, ENNZ liners was subsequently adapted to the creation of an array of compact resonant apertures demonstrating extraordinary transmission (EOT) well below their natural aperture resonances, but without reliance on diffraction anomalies related to the aperture period, as would be observed in more traditional EOT scenarios.

2.4. *Transmission-line metamaterial*

The thin wire and split ring resonator have limited practical applications because these structures are exhibit high loss and narrow bandwidth. A solution was identified by recognizing that the well-known transmission line (TL) theory models transverse electromagnetic wave propagation in a material using distributed lumped elements. In conventional materials, the use of per-unit-length series inductance and shunt capacitance represent positive permeability and permittivity respectively. It was observed by Iyer and Eleftheriades [43] and Caloz *et al.* [44, 45] that loading a host TL medium at subwavelength intervals in an inverted fashion, i.e. using discrete series capacitors and shunt inductors, would result in backward-wave (or left-handed) propagation over a finite, yet broad, bandwidth described by a negative phase velocity or, equivalently, a negative refractive index (NRI). As such, these TL metamaterials, which exhibited properties inherited from both the underlying TL and the periodic reactive loading, came to be known as NRI-TL metamaterials or composite right-/left-handed (CRLH) TL metamaterials.

3. Rectangular and parallel-plate waveguides

In this section, we first analyze the parallel-plate waveguide made of two infinitely extended PECs which are separated by a distance d $(= d_1 + d_2)$ as shown in Figure 2(a). The slab consisting of space in between can constitute different pairs of positive and negative relative permittivity and permeability. The transverse wave number is always imaginary for the propagating modes, when the slab is made of $\varepsilon_1 < 0, \mu_1 > 0$ and $\varepsilon_2 > 0, \mu_2 < 0$ materials or vice versa. But the transverse wavenumber can be real or imaginary depending on the wavenumber in the direction of wave of propagation, when the slab is made of a negative index material ($\varepsilon_1 < 0, \mu_1 < 0$) and a positive index material ($\varepsilon_2 > 0, \mu_2 > 0$) materials or vice versa. The dispersion relation for the TE and TM modes in the parallel-plate waveguide are

$$\frac{\mu_1}{k_1} \tan(k_1 d_1) = -\frac{\mu_2}{k_2} \tan(k_2 d_2); \quad \frac{\varepsilon_1}{k_1} \cot(k_1 d_1) = -\frac{\varepsilon_2}{k_2} \cot(k_2 d_2), \tag{5}$$

respectively. Where $k_i = \sqrt{(\omega^2 \varepsilon_i \mu_i - \beta^2)}$, for $i = 1, 2$ and β is the wave propagation constant in the direction of propagation of the wave (along the x-direction). From the dispersion relations (5), it is found that if the values of μ_1 and μ_2 have the same sign then the TE mode has no real value of the propagation constant. Similarly, for the TM mode with the same sign of value of ε_1 and ε_2, there is no propagation. The parallel-plate waveguide shows an interesting resonance when one slab of the parallel plate waveguide is made up with epsilon negative ($\varepsilon < 0, \mu > 0$) (ENG) and the other slab has mu negative ($\varepsilon > 0, \mu < 0$) (MNG) [15]. Here, it is also noted that no interface can support both TE and TM modes of propagation [15]. Due to the monotonic behaviour of the hyperbolic tangent function in the dispersion equation, for every pair of values of d_1 and the
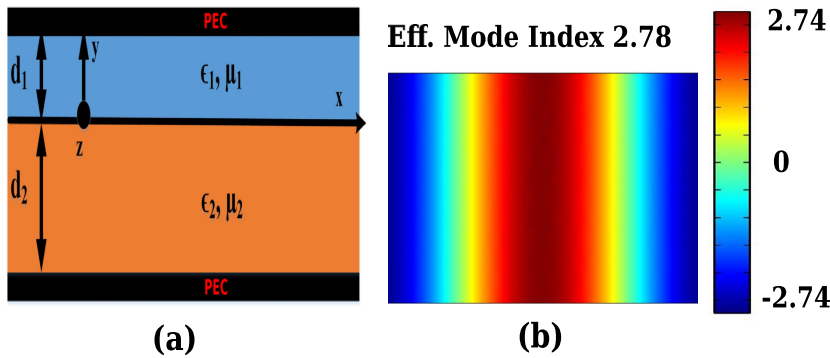
Figure 2. (a) Schematic diagram of a parallel plate waveguide filled with metamaterial slabs. (b) Axial magnetic field components showing the propagation of the $TE_{0,1}$ mode in a homogeneously-filled rectangular waveguide (35 mm × 16 mm) at 3 GHz (below the cutoff frequency), where the permeability tensor is taken to be $(-1.2, 1.1, 1.1)$.

wave propagation constant, there is a unique value of d_2. In a double positive index material slab, multiple solutions of d_2 occur due to the periodic behaviour of fields. This is a unique characteristic of the parallel-plate waveguide made of ENG, and MNG materials. The detailed analysis of the parallel-plate slab waveguide is available in Refs. [15, 46, 47].

The conventional slab waveguide can act as a nonleaky waveguide for electromagnetic waves provided the refractive index of slab is higher than the surrounding dielectric medium. A slab waveguide made up of a negative refractive index material surrounded by a positive index medium has some novel properties such as the absence of fundamental modes [18]. The detailed analysis of an isotropic and an anisotropic slab waveguide is available in Refs. [18, 48–50].

3.1. *Anisotropic rectangular waveguide*

Xu *et al.* theoretically considered a rectangular waveguide filled with an anisotropic metamaterial and derived the general conditions for propagating TE and TM modes [51]. It was found that modes exist that propagate at low frequencies with cutoff at high frequencies [51]. Hrabar *et al.* demonstrated backward-wave propagation in miniaturized-transverse-dimension rectangular waveguides filled with an anisotropic metamaterial having a tensorial negative permeability [52]. All the walls of the rectangular waveguide are made up with PECs and the negative permeability is generated in by placing SRR structures parallel to the side walls of the waveguide. The distance between the SRRs is very small compared to the wavelength of radiation. We assume that the direction of propagation and the axis of waveguide are along the z-axis. The permeability tensor becomes (μ_t, μ_l, μ_l), where the values of μ_t and μ_l can be negative and positive, respectively, when the waveguide is filled with SRRs parallel to the side walls. This structure can support backward waves below the cutoff frequency of the dominant TE mode of the waveguide filled with a uniaxial material with negative permeability (other permittivity and permeability components are positive). All TE modes are backward waves below the natural cutoff frequency and exhibit low-pass behaviour. The transverse dimensions of this waveguide can be much smaller than the free space half-wavelength of the propagating wave. As the negative permeability only has a limited frequency band, this waveguide behaves as a band pass filter with central frequency located below the natural cutoff frequency of the waveguide [52,53]. The propagation of the $TE_{0,1}$ mode below the natural cutoff frequency is shown in Figure 2(b).
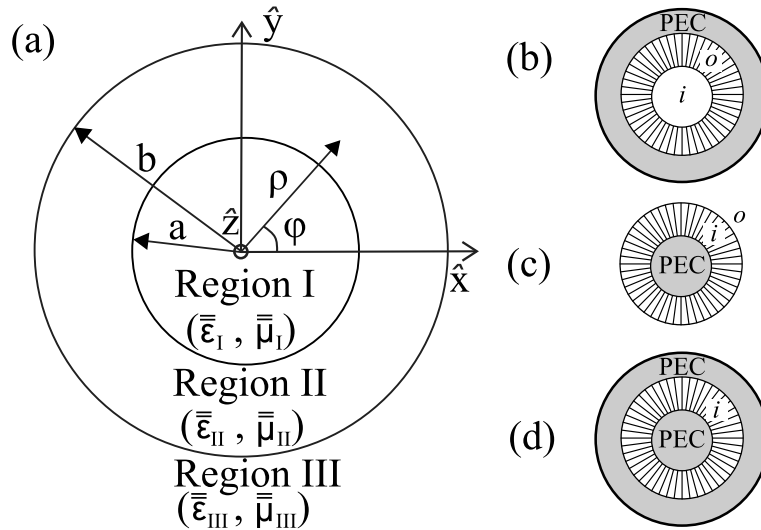
Figure 3. (a) Three-region waveguide setup for the following cases: (b) a metamaterial-lined PEC cylindrical waveguide, (c) a metamaterial-coated PEC rod, and (d) a metamaterial-filled coaxial waveguide. In all cases, the metamaterial region is represented using radial lines. Reprinted from [59], with the permission of AIP Publishing.

A similar planar/rectangular waveguide filled with SRRs was considered in Ref. [54], where modes with no cutoff were investigated. Slow-wave propagation of the guided modes was highlighted and the bianisotropy of SRR media was also considered. Meng *et al.* also theoretically considered an anisotropic metamaterial-filled rectangular waveguide and deduced the presence of both forward and backward propagation as well as forward-wave propagation below the conventional cutoff condition [55]. A giant modal birefringence was theoretically reported in Ref. [56] for a rectangular waveguide filled with a hyperbolic metamaterial at THz frequencies. Polarization effects and manipulation by using the large modal birefringence between the TE and TM modes was highlighted, and it was shown that the waveguide could act as a polarizer or a waveplate. A 50-fold enhancement of the spontaneous emission from molecules embedded in a slab of gold nanowire was reported in Ref. [57], where the emission coupled strongly to the waveguide modes and showed strong polarization effects due to preferential coupling. Ref. [58] presents a theoretical investigation of extraordinary transmission of light through a rectangular waveguide filled with an extreme uniaxial metamaterial having $\varepsilon_z \to \infty$ and $\mu_z \to \infty$, where z is the axis of the waveguide. It was concluded that a large number of higher-order guided modes propagate within the waveguide well below the conventional cutoff.

4. Cylindrical waveguides

In this section, we treat a class of anisotropic cylindrical waveguides consisting of 3 concentric regions (see Figure 3(a)): a central inner core region I of radius a, surrounded by an outer region II of radius b, embedded in a background medium III. Three distinct structures are considered: the metamaterial-lined PEC waveguide (Figure 3(b)), the metamaterial-coated PEC rod (Figure 3(c)), and the metamaterial-filled coaxial waveguide (Figure 3(d)).

Travelling-wave solutions along the axis of the waveguide are assumed. The metamaterial may be isotropic or anisotropic, but usually the cladding or core regions are taken to be isotropic. If an anisotropic core is considered, then at the centre the anisotropy can not be defined due to the

geometrical singularity in the cylindrically symmetric medium. Hence we have to always exclude the centre of the anisotropic metamaterial waveguide by including a PEC boundary condition near the centre or by including an isotropic core at the centre.

4.1. *Analysis of the modes in a cylindrical waveguide*

Let's consider a cylindrically symmetric anisotropic medium whose permitivity and permeability are given by the diagonalised tensors $\bar{\bar{\varepsilon}} = (\varepsilon_r, \varepsilon_\phi, \varepsilon_z)$ and $\bar{\bar{\mu}} = (\mu_r, \mu_\phi, \mu_z)$, respectively. Travelling-wave solutions are considered in the cylindrically symmetric medium as,

$$\vec{E}(r, \phi, z, t) = \vec{E}(r, \phi) e^{i(\beta z - \omega t)}, \tag{6a}$$

$$\vec{H}(r, \phi, z, t) = \vec{H}(r, \phi) e^{i(\beta z - \omega t)}, \tag{6b}$$

where β is the propagation constant along the z-direction. Inserting these (6) in the Maxwell's equations, the transverse components of the electric and magnetic fields can be written in terms of the longitudinal components as,

$$E_r = \left\{ \frac{i\omega\mu_0\mu_\phi}{\omega^2\varepsilon_0\mu_0\varepsilon_r\mu_\phi - \beta^2} \right\} \left(\frac{\beta}{\omega\mu_0\mu_\phi} \frac{\partial E_z}{\partial r} + \frac{1}{r} \frac{\partial H_z}{\partial \phi} \right), \tag{7a}$$

$$E_\phi = \left\{ \frac{i\omega\mu_0\mu_r}{\omega^2\varepsilon_0\mu_0\varepsilon_\phi\mu_r - \beta^2} \right\} \left(-\frac{\partial H_z}{\partial r} + \frac{\beta}{\omega\mu_0\mu_r} \frac{1}{r} \frac{\partial E_z}{\partial \phi} \right), \tag{7b}$$

$$H_r = \left\{ \frac{i\beta}{\omega^2\varepsilon_0\mu_0\varepsilon_\phi\mu_r - \beta^2} \right\} \left(\frac{\partial H_z}{\partial r} - \frac{\omega\varepsilon_0\varepsilon_\phi}{\beta} \frac{1}{r} \frac{\partial E_z}{\partial \phi} \right), \tag{7c}$$

$$H_\phi = \left\{ \frac{i\beta}{\omega^2\varepsilon_0\mu_0\varepsilon_r\mu_\phi - \beta^2} \right\} \left(\frac{\omega\varepsilon_0\varepsilon_r}{\beta} \frac{\partial E_z}{\partial r} + \frac{1}{r} \frac{\partial H_z}{\partial \phi} \right). \tag{7d}$$

In general, the modes will be hybrid EH or HE. But for the special cases $H_z = 0$ the modes will be transverse magnetic (TM) and $E_z = 0$ the modes will be transverse electric (TE). This will happen in the case (3) of a coaxial waveguide.

By putting E_r and E_ϕ from (7a) and (7b) in the Maxwell's curl equation for electric field, we obtain

$$\frac{\omega\mu_0}{r} \frac{\partial}{\partial r}\left(\frac{\mu_r}{q} r \frac{\partial H_z}{\partial r} \right) + \chi \frac{\beta}{r} \frac{\partial^2 E_z}{\partial r \partial \phi} + \frac{\omega\mu_0\mu_\phi}{p} \frac{1}{r^2} \frac{\partial^2 H_z}{\partial \phi^2} - \frac{\beta}{r} \frac{\partial}{\partial r}\left(\frac{1}{q} \right) \frac{\partial E_z}{\partial \phi} + \omega\mu_0\mu_z H_z = 0. \tag{8}$$

Putting H_r and H_ϕ from (7c) and (7d) in the Maxwell's curl equation for magnetic field, we get

$$\frac{\omega\varepsilon_0}{r} \frac{\partial}{\partial r}\left(\frac{\varepsilon_r}{p} r \frac{\partial E_z}{\partial r} \right) + \chi \frac{\beta}{r} \frac{\partial^2 H_z}{\partial r \partial \phi} + \frac{\omega\varepsilon_0\varepsilon_\phi}{q} \frac{1}{r^2} \frac{\partial^2 E_z}{\partial \phi^2} + \frac{\beta}{r} \frac{\partial}{\partial r}\left(\frac{1}{p} \right) \frac{\partial H_z}{\partial \phi} + \omega\varepsilon_0\varepsilon_z E_z = 0. \tag{9}$$

In (8), and (9), we have defined

$$p = \frac{\omega^2}{c^2}\varepsilon_r\mu_\phi - \beta^2, \quad q = \frac{\omega^2}{c^2}\varepsilon_\phi\mu_r - \beta^2, \quad \chi = \left(\frac{1}{p} - \frac{1}{q} \right). \tag{10a}$$

Equations (8) and (9) are coupled to each other and are difficult to solve for an anisotropic and inhomogeneous case. For the anisotropic and homogeneous case, the problem is solvable. For the TE modes, the obtained solutions within the anisotropic medium defined entirely by the H_z component, are

$$H_z = [A_{\text{TE}} J_\nu(k_{\text{TE}}r) + B_{\text{TE}} Y_\nu(k_{\text{TE}}r)] \exp[i(m\phi + \beta z)], \tag{11}$$

where J_ν and Y_ν are the Bessel and Neumann functions of order ν, and m is a non-zero integer. To simplify, if one considers only dielectric anisotropy with $\mu = 1$, and $\varepsilon_z = \varepsilon_\phi$, we have

$$k_{\text{TE}}^2 = \varepsilon_\phi \frac{\omega^2}{c^2} - \beta^2, \quad \text{and} \quad \nu^2 = \frac{(\varepsilon_\phi\omega^2/c^2 - \beta^2)}{(\varepsilon_r\omega^2/c^2 - \beta^2)} m^2. \tag{12}$$

Table 1. Table showing the conditions on the material parameters and the propagation constant to obtain imaginary orders (v or τ) for the Bessel functions that describe the modes for the TE and TM polarizations in the anisotropic fiber

Mode	k_{TE} or k_{TM}	Conditions for k_{TE} or k_{TM}	Requirements for $v^2 < 0$ or $\tau^2 < 0$
TE	Real	$\varepsilon_\phi > \beta^2/k_0^2$	$\varepsilon_r < \beta^2/k_0^2 < \varepsilon_\phi$
	Imag.	$\varepsilon_\phi < \beta^2/k_0^2$	$\varepsilon_\phi < \beta^2/k_0^2 < \varepsilon_r$
TM	Real	$\varepsilon_z/\varepsilon_r > 0, \varepsilon_r > \beta^2/k_0^2$	$\varepsilon_\phi/\varepsilon_r < 0, \varepsilon_r > \beta^2/k_0^2, \varepsilon_\phi > \beta^2/k_0^2$
			$\varepsilon_\phi/\varepsilon_r > 0, \varepsilon_\phi < \beta^2/k_0^2 < \varepsilon_r$
		$\varepsilon_z/\varepsilon_r < 0, \varepsilon_r < \beta^2/k_0^2$	$\varepsilon_\phi/\varepsilon_r < 0, \varepsilon_r < \beta^2/k_0^2, \varepsilon_\phi < \beta^2/k_0^2$
			$\varepsilon_\phi/\varepsilon_r > 0$ and $\varepsilon_r < \beta^2/k_0^2 < \varepsilon_\phi$

Note that $k_0^2 = \omega^2/c^2$.

An analogous expression is obtained for the TM modes, defined entirely by the E_z component, are

$$E_z = [A_{\text{TM}} J_\tau(k_{\text{TM}} r) + B_{\text{TM}} Y_\tau(k_{\text{TM}} r)] \exp[i(m\phi + \beta z)], \tag{13}$$

where J_τ and Y_τ are the Bessel and Neumann functions of order τ,

$$k_{\text{TM}}^2 = \frac{\varepsilon_z}{\varepsilon_r}(\varepsilon_r \omega^2/c^2 - \beta^2), \quad \text{and} \quad \tau^2 = \frac{\varepsilon_\phi}{\varepsilon_r}\left(\frac{\varepsilon_r \omega^2/c^2 - \beta^2}{\varepsilon_\phi \omega^2/c^2 - \beta^2}\right) m^2. \tag{14}$$

The properties of the modes critically depend on v, τ, k_{TE} and k_{TM}. A few conditions for the TE and TM modes are summarised in Table 1. It is well known in literature of hyperbolic metamaterials [10] that when k_{TE} or k_{TM} is imaginary, modal solutions take the form of the modified Bessel functions. We should note that, in such cases, the anisotropic nature of the waveguide allows the order, v or τ, of the Bessel function to be fractional and sometimes even imaginary ($v^2 < 0$ or $\tau^2 < 0$) [60, 61], which is not possible in the conventional isotropic waveguide. We consider only a propagating (β is real) TE mode with real k_{TE} (implying that $\varepsilon_\phi > \beta^2 c^2/\omega^2$). If $\varepsilon_r < \beta^2 c^2/\omega^2 < \varepsilon_\phi$, then $v^2 < 0$ and the order of the mode becomes an imaginary number. This occurs straightforwardly in a medium with $\varepsilon_r < 0$ and $\varepsilon_\phi > 0$, whereas in a medium with $\varepsilon_r = \varepsilon_\phi$, such a situation would not occur. Note that the inequalities become reversed if we seek a TE mode with imaginary k_{TE} described by the modified Bessel functions. The requirements for an imaginary order of the TM modes represents slightly more cases due to several possibilities of the material permittivity, and Table 1 summarizes these conditions for $\tau^2 < 0$. Some simplifications may occur when $\varepsilon_z = \varepsilon_\phi$ because of the reduced number of constraints in the mathematical expressions.

4.2. *Experimental realizations and applications*

In practice, it has been complicated to organize metamaterial structures within the small confines of a waveguide. When the waveguide size is large, such as in the case of structures at tens of MHz for MRI, it is possible to organize such structures. For high frequency solutions, such as at optical IR frequencies, the small micro and nanosizes demand approaches involving self-organization processes. Very few such metamaterial waveguides have been experimentally realised and many are yet to be properly explored. In general, we can categorize the waveguides into three kinds: axial structuring, radial structuring and metamaterial-clad waveguides. Here we will discuss a few cases of cylindrical waveguides that have been experimentally realized.
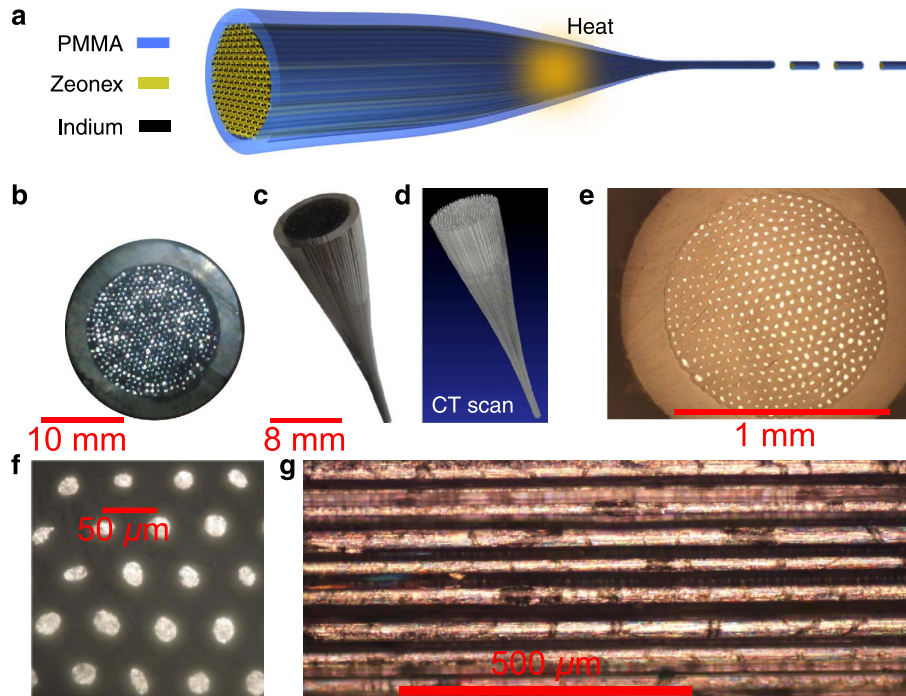
Figure 4. (a) Schematic plan and drawing of the fiber, (b) Optical photograph of the cross-section. (c) Optical and (d) Computed Tomography (CT) scan image of the tapered region. (e) 10 times zoomed optical microscope image of the cross-section, (f) 40 times zoomed image and (g) longitudinal optical microscope image of the waveguide. Figure reproduced from [64]; Licensed under Creative Commons Attribution-NonCommercial-ShareAlike 3.0 Unported License (CC BY-NC-SA 3.0).

4.2.1. *Axially structured waveguide*

This type of waveguide is typically axially invariant and usually has an axially continuous structure. These waveguides also show anisotropy of the type $\varepsilon_r = \varepsilon_\phi \neq \varepsilon_z$. Such metamaterial waveguides are typically fabricated by fiber-drawing techniques [62, 63]. Figure 4 shows the schematic and optical microscope images of such an example. By stacking indium metal wires in a low-absorption polymer Zeonex, a preform of 1 cm is created in a polymethyl methacrylate (PMMA) tube [64]. This assembly is heated whereby the polymer becomes viscous and metal becomes liquid, so that the preform can be drawn from a tapered die into a uniform fiber. The choice of indium here is to match the low-temperature softening behaviour of PMMA. The cross-section of the waveguide and its optical microscope images are shown in other sub-figures.

These waveguides have been used for imaging and focusing of terahertz (THz) radiation at the below the diffraction limit. Figure 5 shows the experimental and simulated results of the intensity from the two apertures made of 50-μm-thick brass discs. The diameter, separated inner-edge, and length of this metamaterial waveguide are 200 μm, 100 μm, and 3.4 mm, respectively. Here the intensity is a function of the position and frequency averaged at the centre plane ($y = 0$). The direct near-field measurement of the apertures without the waveguide is also shown for comparison. Panels 5(a–d) show the output intensity measurement of the apertures without the waveguide. It is clear that even measuring just after the apertures at a 125 μm distance from the apertures there is diffraction in the images. Panels 5(e–h) show the aperture output intensity after
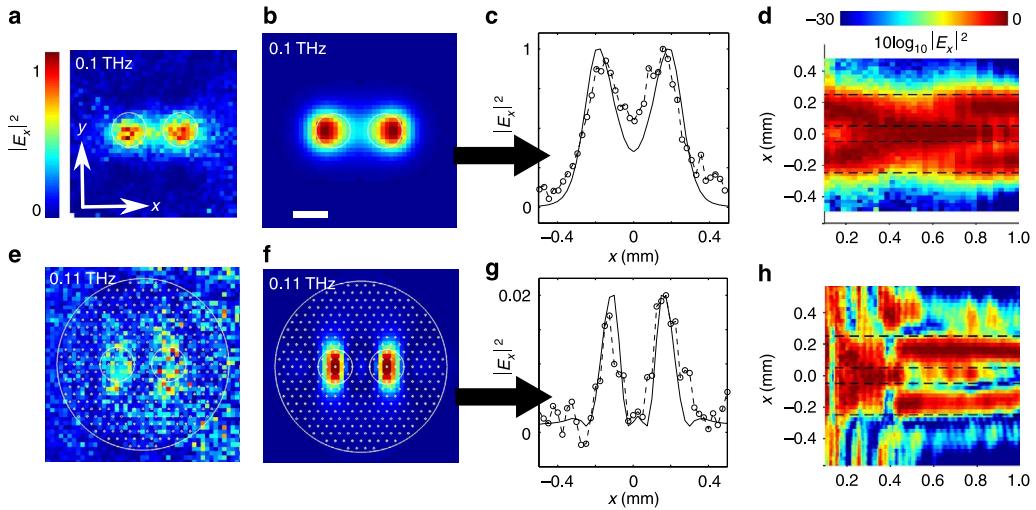
Figure 5. (a) Measured and (b) simulated intensity of two apertures of 200 μm diameter with separated inner-edge of 100 μm at 0.1 THz frequency was calculated at 125 μm from the output of the aperture, (c) intensity distribution along *x*-direction at $y = 0$ μm, and (d) the logarithmic intensity distribution with respect to the incident frequencies along the *x*-direction averaged over $y = 0 \pm 50$ μm. (e) Measured and (f) simulated intensity of the same apertures propagating through the 3.4 mm long metamaterial waveguide, calculated at 50 μm output from the waveguide, (g) intensity distribution along the *x*-direction, averaged over $y = 0 \pm 100$ μm, and (h) the logarithmic intensity distribution with respect to the incident frequencies along the *x*-direction averaged over $y = 0 \pm 100$ μm. Figure reproduced from [64]; Licensed under Creative Commons Attribution-NonCommercial-ShareAlike 3.0 Unported License (CC BY-NC-SA 3.0).

light travels through the 3.4-mm-long metamaterial waveguide and were measured at a 50 μm distance from the waveguide. Here there is clear evidence that the images are diffraction-free and that resolution is increased. This happens since the wired metamaterial shows hyperbolic dispersion and along the *z*-direction and very large propagation vectors are achieved [9, 10], which focuses both the near-field as well as the far-field. Therefore, diffraction-free images become possible using the metamaterial waveguide.

Another example that can be used is the hollow-core metamaterial waveguide. Min Yan and co-workers theoretically show that a hollow-core metamaterial waveguide made of silver-silica multilayered metamaterial can transport TM IR light 100 times more effectively than a simple hyperbolic metamaterial waveguide [65]. Such a hollow-core waveguide exhibits lower losses than the non-hollow hyperbolic metamaterial fiber. These waveguides can be used for IR applications.

4.2.2. *Radially structured waveguide*

In this type of waveguide, the structuring is perpendicular to the waveguide axis, althrough the invariance along the axis is preserved in a coarsely grained metamaterial description. For example, there can be nanopores or nanowires oriented along the radial direction of the waveguide, in which case the anisotropy is of the type $\varepsilon_r \neq \varepsilon_\phi = \varepsilon_z$. Such a waveguide was first realized by a nanoporous alumina metamaterial waveguide [13, 59, 66, 67]. This nanoporous alumina waveguide consists of an inner impermeable alumina nano layer near the centre from which nanopores
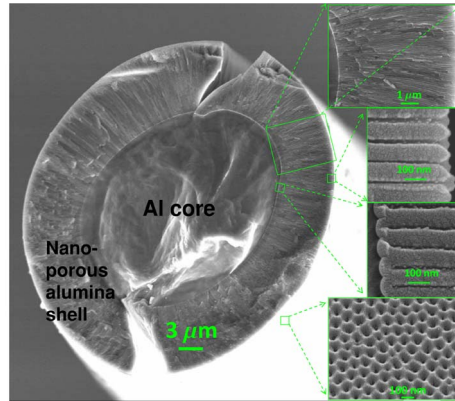
Figure 6. Scanning electron microscope (SEM) image of the nanoporous alumina waveguide. The presence of the radially oriented non-branching nanopores are clearly shown. The nanoporous outer surface and the impermeable barrier pure alumina oxide layer at the inner tubular surface are shown in the insets. Brittle alumina waveguides crack when cleaved for SEM imaging. Reprinted with permission from [13] © The Optical Society.

radially emanate and terminate at the outer nanoporous surface formed by the nanopores, as shown in Figure 6. The nanopores of this waveguide may be filled with a plasmonic metal like silver, gold etc. by electrodeposition techniques [24]. This results in an extremely large anisotropy in the waveguide. In this case, the centre of the waveguide has an aluminum core (PEC) or an impermeable alumina core (isotropic medium). A local Maxwell–Garnett or Bruggeman homogenization process can be adopted to describe the effective medium permittivity at each point locally. This has also been validated by a geometric mapping of the cylindrical system to a planar system [13].

The guiding of light through a bent section of a nanoporous anisotropic waveguide and an aluminium core is shown in Figures 7(a,b). The scattering from the structure and other defects is strong, but the evidence for the light confinement and guidance is very clear. Because of the large scattering, most of the modes get coupled, and it was not possible to image the mode structure of the propagating modes. The propagation losses will also be very large due to the structured nature. Figures 7(c,d) show the variation in the anisotropic material effective permittivity with radial distance calculated for air nanopores in the cylindrical nanoporous alumina, and silver nanowires in nanoporous alumina where a Drude dielectric permittivity model for silver was used, given by $\varepsilon_{Ag} = \varepsilon_{\infty} - \omega_p^2/[\omega(\omega + i\gamma)]$ with $\varepsilon_{\infty} = 5.7$, $\omega_p = 9.2$ eV and $\gamma = 0.021$ eV [68]. The host alumina data is available in Ref. [69]. The imaginary part of the effective permittivity for the silver-nanowires-filled nanoporous structure is also small due to the small fill fractions. Because of the radial variation of the nanopores, the nanoporous alumina waveguides are actually spatially inhomogenous, which will affect the nature of the modes. Figures 7(e, f) show the normalized electric field (E_z) plots of two TM modes for homogeneously filled metamaterial waveguides. The modes of the plots intentionally used high m value (40) to show the effect of the imaginary order (τ). If the effective order τ value is real but fractional then for high m, the field is pushed outwards from the centre of waveguide, but when the effective τ is imaginary then the field is concentrated towards the centre of the waveguide.

Another good example of a radially structured metamaterial waveguide is a hybrid-glass metamaterial fiber, which was reported for nonlinear effects [70]. This waveguide is fabricated by a laser-based fiber drawing technique [71, 72]. To fabricate such a waveguide, sapphire ($\alpha - Al_2O_3$)

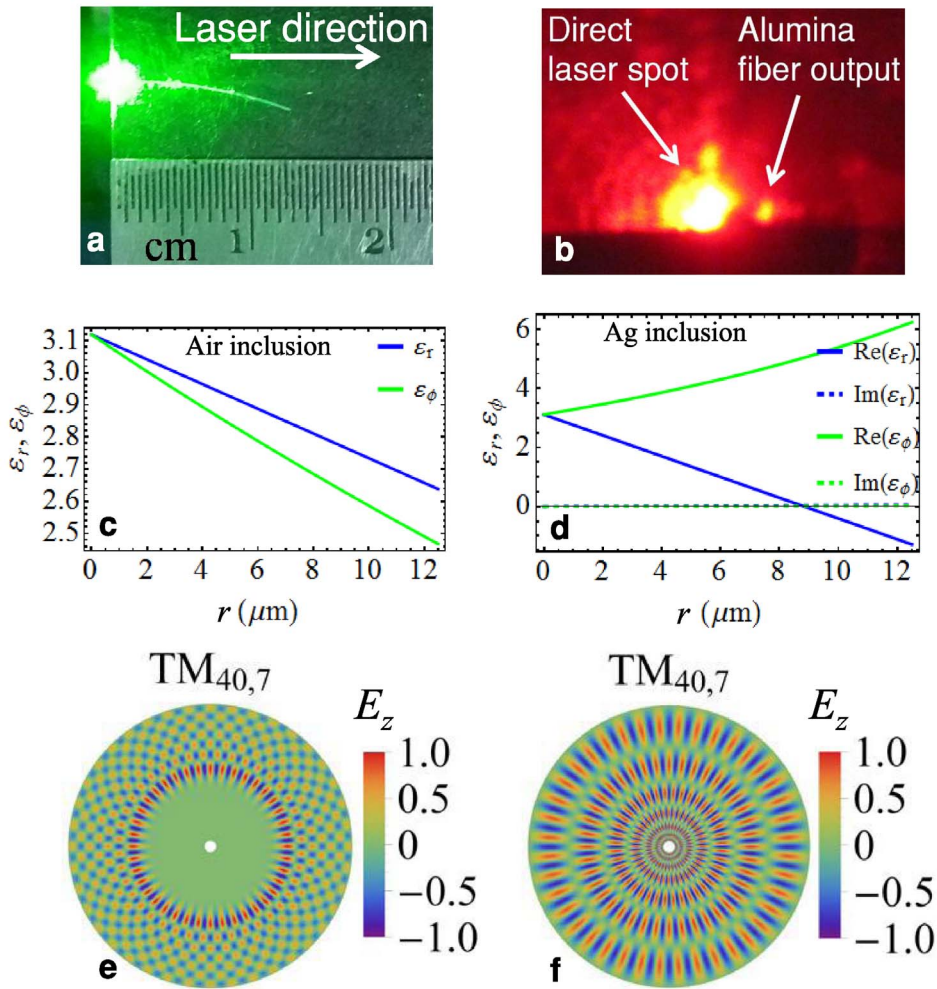**Figure 7.** (a) Picture of light (λ = 532 nm) propagating across a bent nanoporous alumina waveguide with an aluminum core (Aluminium core diameter—10 µm, nanoporous alumina shell diameter—80 µm, length—1.3 cm, nanopore diameter is 30 nm and nanopore periodicity is 100 nm at outer surface). (b) The light output from the waveguide at λ = 633 nm. Plots of the variation of the effective dielectric permittivity components with the radial distance in a nanoporous alumina waveguide for (c) air inclusion, and (d) when the nanopores of the waveguide are filled with silver nanowires for nanopore radius q = 25 nm at outer surface and f = 0.23. The bottom: Calculated normalized electric field (E_z) plots of TM modes for homogeneously filled coaxial metamaterial waveguides at λ = 633 nm, (e) for fractional order modes when ε_r = 2.467 and $\varepsilon_\phi = \varepsilon_z$ = 2.638, and (f) for imaginary order modes when ε_r = 2.638 and $\varepsilon_\phi = \varepsilon_z$ = 2.467. Reprinted with permission from [13] © The Optical Society.

was taken as a seed dielectric core and dendrite crystalline $\gamma - Al_2O_3$ was deposited on it. A silica layer is coated on the outside as a cladding. Such a waveguide is used for second harmonic generation (SHG) using nonlinear effects. This waveguide has monolithically integrated dendrites for intracavity and resonant SHG. Similar to the nanoporous fiber developed by anodization and

Table 2. Table showing the dependence of the axial propagation constant (β), cutoff frequency and order of the propagating modes with the material parameters

Mode	Material permittivity ($\mu = 1$)	Axial propagation constant (β)	Remarks about modes and cutoff frequencies
TE	$\epsilon_r < 0; \epsilon_\phi > 0; \epsilon_z > 0$	$\sqrt{k_0^2 \, |\epsilon_\phi| - k_{\text{TE}}^2}$	Finite cutoff, solutions similar to positive index fibers, Modes may be fractional order or Imaginary order
TE	$\epsilon_\phi < 0; \epsilon_r > 0; \epsilon_z > 0$	$i\sqrt{k_0^2 \, |\epsilon_\phi| + k_{\text{TE}}^2}$	No propagation
TE	$\epsilon_z < 0; \epsilon_r > 0; \epsilon_\phi > 0$	$\sqrt{k_0^2 \epsilon_\phi - k_{\text{TE}}^2}$	Finite cutoff, solutions similar to positive index fibers, Modes may be fractional order or Imaginary order
TM	$\epsilon_r < 0; \epsilon_\phi > 0; \epsilon_z > 0$	$i\sqrt{k_0^2 \, |\epsilon_r| - \frac{|\epsilon_r|}{\epsilon_z} k_{\text{TM}}^2}$	Upper cutoff, Mode has upper limitation of frequencies for propagation, modes may be imaginary order
TM	$\epsilon_\phi < 0; \epsilon_r > 0; \epsilon_z > 0$	$\sqrt{k_0^2 \epsilon_r - \frac{\epsilon_r}{\epsilon_z} k_{\text{TM}}^2}$	Finite cutoff, solutions similar to positive index fibers, modes may be fractional order or imaginary order
TM	$\epsilon_z < 0; \epsilon_r > 0; \epsilon_\phi > 0$	$\sqrt{k_0^2 \epsilon_r + \frac{\epsilon_r}{|\epsilon_z|} k_{\text{TM}}^2}$	No cutoff frequency, modes may be fractional order or imaginary order

electrodeposition techniques, the laser-based fiber drawing technique also results in a volumetric metamaterial waveguide that can be rapidly fabricated over large lengths.

4.3. *Modes and applications of hyperbolic waveguides*

The waveguide filled with hyperbolic metamaterials has advantageous propagation properties. The axial propagation constant, cutoff frequencies and the order of propagating modes are shown in Table 2 for different hyperbolic permittivity tensors by using the dispersion equations (14). It is seen that the radial and axial hyperbolic metamaterial waveguides have no cutoff frequencies for the transverse magnetic modes. The propagation of modes much below the cutoff frequency was verified by an explicit calculation using the COMSOL® Multiphysics Simulation Suite based on the finite element method. The fields of these eigenmodes are shown in Figure 8 for a waveguide with $\epsilon_r = -1$, $\epsilon_\phi = \epsilon_z = 3.2883$, and inner and outer diameters of 200 nm and 500 nm, respectively. The real positive values of effective mode indices are evidence of forward propagating modes at 200 THz, much below the natural cutoff frequency (the minimum cutoff frequency to propagate the TM_{11} mode in an equally size waveguide filled with an isotropic medium is 567.8 THz), as shown in Figure 8.

This can be advantageously used to couple the near-field evanescent modes associated with large transverse wavevectors of small sources to these high-angular-momentum waveguide modes, well below the conventional cutoff frequencies [16]. Such waveguides can couple light very efficiently from small sources into the propagating modes of the waveguide, which can then
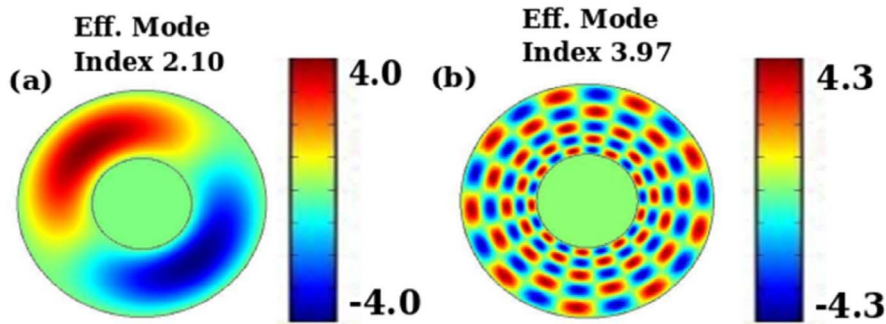
Figure 8. Electric fields (E_z) in an anisotropic hyperbolic fiber, when the annular region ($R_1 < r < R_2$) has $\epsilon_r^{\mathrm{eff}} = -1, \epsilon_\phi^{\mathrm{eff}} = \epsilon_z^{\mathrm{eff}} = 3.2883$, $R_1 = 100$ nm and $R_2 = 500$ nm. The propagating TM_z modes are (a) $TM_{1,1}$ and (b) $TM_{9,5}$ at a frequency of 200 THz.

be adiabatically coupled into a conventional waveguide or fiber. Abhinav *et al.* studied the capability of such a hyperbolic waveguide to transmit power from the near field of subwavelength sources, where the inner and outer surfaces of the annular region of the waveguide (as shown in region II of Figure 3(a)) is covered with air and PEC respectively [16]. They found that the average power at the output port is higher for the radial hyperbolic case ($\epsilon_r < 0; \epsilon_\phi \simeq \epsilon_z > 0$) by several orders of magnitude compared to the angular hyperbolic ($\epsilon_\phi < 0; \epsilon_r \simeq \epsilon_z > 0$) and the axial hyperbolic ($\epsilon_z < 0; \epsilon_r \simeq \epsilon_\phi > 0$) cases from a point dipole source at 200 THz. The coupling efficiencies with such an anisotropic waveguide coupler, measuring a few wavelengths long, can exceed the coupling efficiencies with a conventional coupler by a factor of 10^7 [16, 73]. Coupling efficiencies of the radial hyperbolic waveguides are higher when compared with the tapered nanofibers [16]. The radial hyperbolic waveguide can be used as a near-field coupler or an imaging probe, and it has the convenience of butt-coupling, which results in better spatial accuracy.

4.4. *Metamaterial-clad waveguide*

The cladding of a waveguide affects the properties of the waveguide and directly controls the wave propagation within. By changing the cladding, one can vary the electromagetic properties of the waveguide. In the conventional waveguide the cladding is isotropic, but by using an anisotropic metamaterial cladding some unusual properties can be achieved. Metamaterial-clad waveguides show properties like backward propagation below the cut-off frequency with respect to the un-clad waveguide, field collimation [17], miniaturization and resonant tunnelling [74, 75], transport of large amounts of power [76], and slow light propagation [12]. Several metamaterial-clad waveguides have been reported. These claddings are made of many kinds of metamaterial-like subwavelenth layered structures [77], split-ring-resonators [17, 74, 75], microwires or nanowires [65, 67], liquid crystals, or a combinations of these [76, 78]. Metamaterial-clad waveguides are more popular because they are easy to fabricate compared to volume-filled metamaterial waveguides. Due to the large dissipation in metamaterials, metamaterial-clad waveguides may offer better propagation characteristics.

4.5. *Metamaterial-lined PEC waveguide*

First, the practical realization of an ENNZ-metamaterial-lined waveguide is discussed. To realize the ENNZ-metamaterial liner, TL-metamaterials are used.
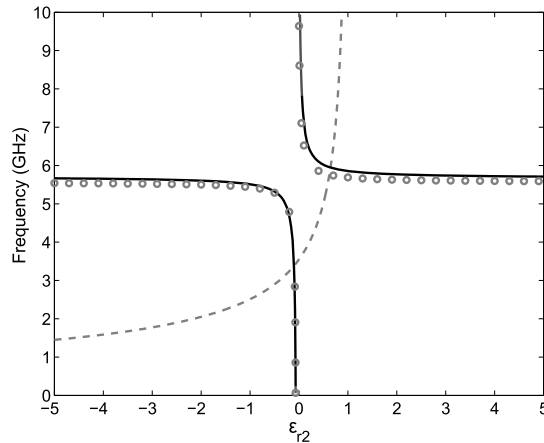
Figure 9. HE$_{11}$ mode cutoff frequency versus liner permittivity. Full, anisotropic dispersion (black curve), approximate isotropic dispersion (empty grey circles), and Drude permittivity model (dashed grey curve). © 2013 IEEE. Reprinted, with permission, from [17].

Experimentally, metamaterials have been incorporated into many devices, including antennas, lenses, couplers, and waveguides. Of interest here is the ENNZ-lined cylindrical waveguide. The ENNZ-lined cylindrical waveguide consists of a metamaterial-lined (and otherwise hollow) PEC cylinder, where the metamaterial is designed to exhibit ENNZ properties, see Figure 3(b). In this case, the ENNZ metamaterial is designed specifically to interact with the HE$_{11}$ mode of the inhomogeneously filled waveguide system as this mode exhibits many desirable properties: below-cutoff propagation and collimated central fields, to name just two. To design a metamaterial that responds in the expected way, consider just the liner region of the waveguide. For the desired HE$_{11}$ mode, the liner exhibits longitudinally directed H-fields and radially directed E-fields. The transverse fields resemble an azimuthal TL-mode standing-wave field distribution. As such, the TL-metamaterial is an ideal metamaterial technology with which to imbue the liner region with ENNZ properties. This can be achieved using the plasma-like properties of an array of thin, highly inductive wires, which exhibits a Drude-like permittivity response near its resonance (plasma) frequency. Thin-wire metamaterials, or equivalently, inductively loaded TL-metamaterials, are generally anisotropic, however, the theoretical analysis above has shown that for a thin liner, the HE$_{11}$ modal cutoff frequency is only weakly dependent on liner properties other than the radial permittivity ϵ_ρ. A representative Drude dispersion curve is plotted against the HE$_{11}$ mode cutoff frequency in Figure 9. Note that the two curves cross at two points: the first at $f = 3.381$ GHz, and second at $f = 5.958$ GHz. The first corresponds to the designed ENNZ region with $\epsilon_{r2} = -0.09$ and is well below the natural TE$_{11}$ cutoff frequency of $f = 5.864$ GHz, while the second corresponds to a nearly homogeneous waveguide with $\epsilon_{r2} = 0.644$, and a cutoff frequency only marginally above the homogeneous waveguide cutoff. A suitable TL-metamaterial to realize the above properties employs an azimuthally directed coplanar-strip (CPS) TL loaded at 45° intervals using discrete inductors to create the ENNZ response. The EH$_{01}$ mode also necessarily exists in the frequency-reduced regime below the liner's plasma frequency, but is orthogonal to the HE$_{11}$ mode and may therefore be suppressed through proper excitation. In addition, higher-order azimuthal resonances may be suppressed by loading the series branch of the CPS TL using a small series capacitance.

   The experimental setup used two shielded-loop antennas to feed a closed cylindrical waveguide, which was either unloaded, or loaded with several printed circuit board rings of the TL-
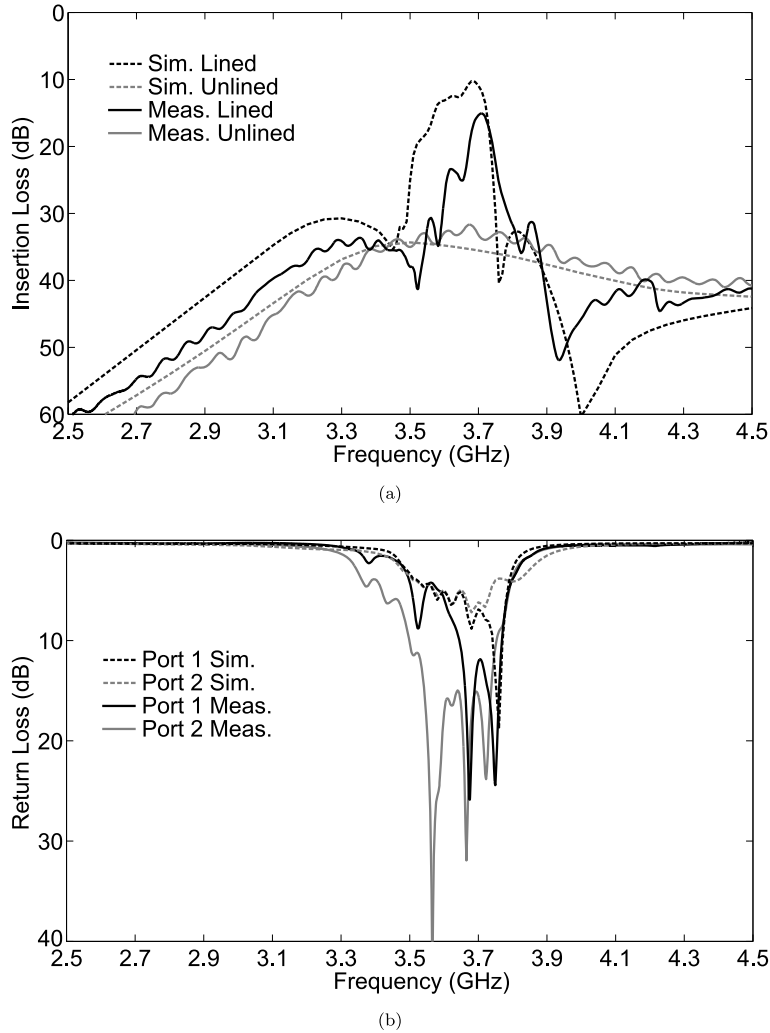
(a)

(b)

Figure 10. (a) Insertion loss and (b) return loss obtained from simulation and measurements of the practical ENNZ-lined metamaterial waveguide. © 2016 IEEE. Reprinted, with permission, from [79].

metamaterial described previously. A comparison of the insertion loss and return loss of the full-wave Ansys high frequency structure simulator (HFSS) simulation to the fabricated structure (see Figure 10) show good agreement and any discrepancies are attributed to fabrication tolerances.

4.5.1. *Applications*

Travelling-wave MRI is a sensing paradigm where the bore of the MRI scanner is treated as a cylindrical waveguide, and the RF signal may be generated/detected by way of externally placed antennas, freeing up space within the bore and also mitigating the problem of standing waves on coils placed within the bore, which can contribute to image dark spots at very high RF frequencies/static field strengths. However, typical human-sized scanners have bore diameters that cause the fundamental TE_{11} mode to be well below cutoff at operating frequencies corresponding

to clinical field strengths, such as 1.5 T or 3 T. In order to restore propagation in such clinical MRI machines and employ the traveling-wave method, it is necessary to somehow reduce the natural cutoff frequency of the bore. Lining the bore of an MRI with an ENNZ-metamaterial liner allows the excitation of the below-cutoff HE_{11} mode to propagate the signal, but the HE_{11} mode also has very homogeneous fields in the central bore, which improves image quality while occupying less space than the conventional birdcage coils that may otherwise induce claustrophobia.

A second application of the ENNZ-lined metamaterial waveguide is particle-beam studies [59]. Specifically, particle-beam studies use the TM_{01} mode of an air-filled cylindrical waveguide to accelerate charged particles to relativistic speeds. Unfortunately, the fundamental mode of a cylindrical waveguide is the TE_{11} mode, thus monomodal operation is impossible and efficiency is degraded. A waveguide lined with a metamaterial that exhibits anisotropic negative and near-zero permittivity supports a spectrum of backward-wave modes, of which the EH_{01} mode has the highest cutoff frequency and hence supports monomodal propagation. This mode also shares many properties with the TM_{01} mode of the unlined cylindrical waveguide, which makes it ideal for the described particle-beam studies. These studies could benefit from increasing the monomodal bandwidth of the EH_{01} mode by reducing the cutoff frequency of the HE_{n1} modes (the first being HE_{11}). The cutoff frequency of the EH_{01} mode occurs at the plasma frequency ω_p of ϵ_ρ of the liner, independent of the other tensor components of ϵ. Further, the cutoff frequency of the HE_{11} mode is reduced for thicker liners. In an illustrative example, it has been shown that the monomodal bandwidth of the EH_{01} mode can be increased by greater than 38.5% over the isotropic case by introducing anisotropy and increasing the liner thickness.

A third application that has been explored is open-ended waveguide probe antennas [74]. Open-ended waveguide (OEWG) probes have many applications, but those that can benefit the most from miniaturization are antenna near-field measurements and material characterization. It was proven that lining an OEWG probe operating below cutoff with an ENNZ-metamaterial liner can improve the gain of the highly miniaturized antenna by over 60 dB.

4.6. *Metamaterial-coated PEC rod*

A PEC rod may be seen as the inverse of the hollow PEC waveguide (Figure 3(c)). The guided modes supported by this structure are tightly bound surface modes referred to as Sommerfeld modes. Recently, these rods have been used as probes in THz-endoscopy methods to sense small quantities of material. These applications use the EH_{01} mode of the rod as it has no cutoff in this geometry and is circularly symmetric. Subwavelength sensing resolution is achieved by tapering the rod to a fine tip. As the field confinement limits the ultimate resolution, the slow-wave, high-β regime is used near the surface plasmon resonance. For smooth metal rods, this occurs at $\omega_{ep}/\sqrt{2}$, where ω_{ep} is the plasma frequency of the bulk metal. Hence, for regular metals, this is a constant frequency range that is often in the UV. At lower frequencies, the required field confinement can be achieved by modifying the plasma frequency through corrugations on the surface of the metal, or by coating the rod in high-permittivity dielectrics. Surface corrugations have been modeled in other contexts using anisotropic surface impedance or by thin layers of anisotropic permittivity and permeability. Here, the EH_{01} mode dispersion is engineered for a rod coated in a thin, practical anisotropic metamaterial [59].

First, consider the case of a metamaterial coating with isotropic permittivity, but chosen plasma frequency ω_{ep}. The dispersion of the EH_{01} mode of this structure closely resembles that of the smooth PEC rod, with field confinement increasing towards ω_{ep}, but the loss introduced by the metamaterial also leads to higher attenuation. Further reduction of the plasma frequency of the metamaterial requires stronger loading components, but this generally increases losses and fabrication difficulty. The dispersion of the EH_{01} mode with anisotropy introduced to the

metamaterial model closely mimics the dispersion of an isotropic EH_{01} with half the plasma frequency, meaning the simple addition of anisotropy effectively halves the lumped component values required to realize the metamaterial. Further, the losses are significantly reduced, and the radial field confinement is improved.

4.7. *Metamaterial-filled coaxial waveguide*

The following section focuses on exploring interesting dispersion phenomena in the THz regime in the recently realized alumina metamaterial-filled coaxial waveguide discussed above, a case of Figure 3(d). The structure consists of an alumina tube embedded with radially emanating micropores, with an aluminum microwire core and finally a thin aluminum outer coating [59].

The dispersion profile of the permittivity tensor for a structure with air-filled pores is weakly anisotropic, and shows strong dispersion where the phonon resonances occur for alumina between 10 and 25 THz. More extreme degrees of anisotropy may be observed by filling the holes with a plasmonic metal such as silver. This frequency regime is well below silver's bulk plasma frequency, hence it exhibits large, negative permittivity. Due to the radial orientation of the nanopores, ϵ_ρ is dominated by the response of the silver, and ϵ_ϕ is marginally affected. Losses are substantially increased.

Next, consider the TM_{11} mode of the coaxial waveguide loaded with the above air-filled porous metamaterial [59]. Above the plasma frequency of 28 THz, the permittivity of the alumina is positive and modal dispersion for the TM_{11} mode approaches what it would be for an isotropic alumina-filled coaxial waveguide, and a low-loss passband occurs. For the isotropic alumina case, near the phononic resonances, (i.e. 13 THz and 17.2 THz), several lossy bands with negative group velocity exist. The introduction of air-filled pores creates a small but lossy backward-wave band between 24 and 25 THz. Finally, the addition of silver into the nanopores severely impacts the mode's dispersion: generally, losses are increased by an order of magnitude, however, a small, low-loss backward-wave band is introduced at 4.3 THz, which may be useful for backward-wave propagation. As the nanopores are hydrophilic, they may be filled with all sorts of materials, such as dye molecules, quantum dots, and dispersed nanoparticles whose resonant features could be used to modify the anisotropic effective permittivity of the waveguide from THz to visible frequencies. The large surface area of the nanopores may also prove beneficial in sensing.

5. From waveguides to apertures

A waveguide may be transformed into an aperture in a few simple steps. Consider again an inhomogeneously filled PEC cylindrical waveguide, as shown in Figure 11: a PEC shell of radius $\rho = b$ is lined with a metamaterial (ϵ_{r2}, μ_{r2}, $a < \rho < b$) and finally filled with air (ϵ_{r1}, μ_{r1}, $\rho < a$) [17]. The PEC condition on the surface of the waveguide enforces that all fields outside the waveguide be zero, thus the PEC wall's thickness may be extended to infinity in the transverse (x–y) plane. This system, of course, supports the same spectrum of modes as the original metamaterial-lined PEC waveguide. Next, shorten the waveguide's extent in the propagation (z-) direction to be infinitesimally small. In this limit, the waveguide becomes an aperture in a PEC sheet, as shown in Figure 12. Apertures in an infinitesimally thin metallic screen support resonances analogous to waveguide modal cutoffs, but do not support guided-wave propagation.

In this section, we begin by exploring the salient features of lining apertures with non-magnetic, epsilon-negative and near-zero (ENNZ) metamaterials by comparing them to equivalent ENNZ-metamaterial-lined waveguides, with examples in both the microwave and optical regimes: the Fano-shape resonant transmission, the waveguide modal cutoff frequency's relation
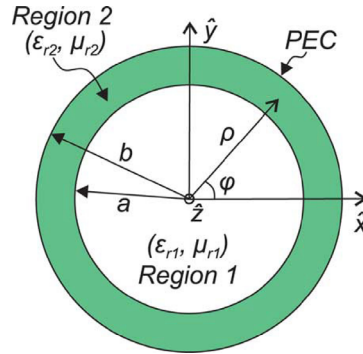
Figure 11. Cross-section of a metamaterial-lined waveguide. Region 1 ($\rho < a$) is filled with vacuum (but may generally take on any ϵ_{r1}, μ_{r1}), region 2 ($a < \rho < b$) is filled with a metamaterial that has arbitrary ϵ_{r2} and μ_{r2}, and the outer boundary at b is a PEC. © 2013 IEEE. Reprinted, with permission, from [17].
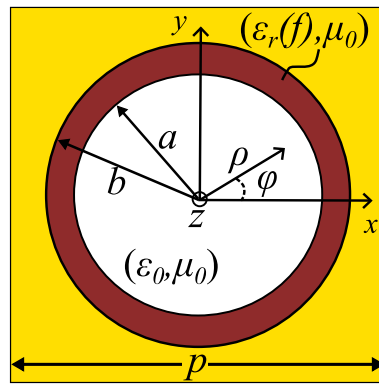

Figure 12. Planar view if an metamaterial-lined aperture. Region 1 ($\rho < a$) is filled with vacuum (but may generally take on any ϵ_{r1}, μ_{r1}), region 2 ($a < \rho < b$) is filled with a metamaterial that has arbitrary ϵ_{r2} and μ_{r2}, and the outer region ($b < \rho$) is a PEC. Reprinted with permission from [80] © The Optical Society.

to the aperture resonance frequency, and the practical implementation. We continue the discussion with an extension into resonant metasurfaces (MTSs), where the ENNZ-metamaterial-lined apertures are arrayed in the transverse plane with period p. This necessitates a discussion on diffraction anomalies, interaperture coupling, and excitation mechanisms. Finally, we conclude with metamaterial-lined aperture MTS applications and outlook.

5.1. *Theory of operation*

Although Bethe's well-known aperture theory predicts that an empty aperture will transmit poorly when it is electrically small (below what would be the cutoff frequency of the equivalent fundamental unlined-waveguide mode), the below-cutoff modes introduced by the metamaterial lining create resonant transmission for subwavelength apertures [80, 81]. This resonance is unlike those most commonly produced by larger apertures as it exhibits a characteristic Fano lineshape, which is a strong enhancement followed by strong extinction of the transmission, as seen in the transmission/reflection parameters plotted in Figure 13.
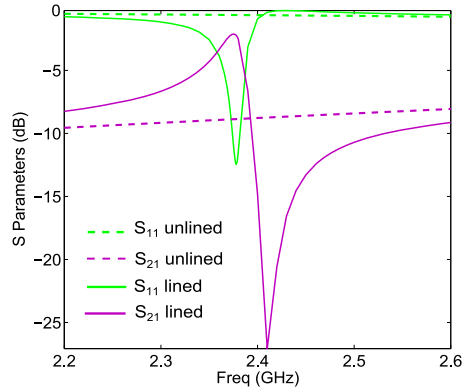
Figure 13. Transmission and reflection parameters of an ENNZ-metamaterial-lined aperture array with $b = 15.65$ mm, $a = 13.69$ mm and $p = 40$ mm (solid). Also plotted is the transmission for an array of apertures with no liner (radius $b = 15.65$ mm and spacing $p = 40$ mm, dashed). Reprinted with permission from [80] © The Optical Society.

The Fano response is well-described by a dual resonator model, under the conditions where a high-Q resonator (i.e. sharp or discrete resonance) interacts with a low-Q resonator spectrum (i.e. wide or continuous spectral response) in the weak-coupling regime [82]. The high-Q resonator has a 180-degree phase shift at resonance, and the wide spectrum follows a continuous phase response. The two constructively then destructively interfere near the discrete resonance frequency to produce the Fano resonance. In the case of the apertures described here, the sharp, frequency-reduced HE_{11} resonance interacts with the low, wide-band background transmission of an unlined aperture predicted by Bethe's theory (the -10-dB unlined transmission shown in Figure 13) to produce a Fano lineshape.

The aperture resonance frequency is very sensitive to the metamaterial liner properties. To find the resonance frequencies, the Helmholtz equation is solved in cylindrical coordinates subject to appropriate boundary conditions, in a similar way to finding the dispersion relation of the equivalent waveguide system, as was done in [79]. The dispersion relation is as follows:

$$A = \left[\frac{\mu_{z1}}{\gamma_{\rho 1}^{\mu}} \frac{J_{\tau 1}'(\gamma_{\rho 1}^{\mu} a)}{J_{\tau 1}(\gamma_{\rho 1}^{\mu} a)} - \frac{\mu_{z2}}{\gamma_{\rho 2}^{\mu}} \frac{G_{\tau 2}'(\gamma_{\rho 2}^{\mu} a)}{G_{\tau 2}(\gamma_{\rho 2}^{\mu} a)} \right] \tag{15a}$$

$$B = \left[\frac{\epsilon_{z1}}{\gamma_{\rho 1}^{\epsilon}} \frac{J_{\nu 1}'(\gamma_{\rho 1}^{\epsilon} a)}{J_{\tau 1}(\gamma_{\rho 1}^{\epsilon} a)} - \frac{\epsilon_{z2}}{\gamma_{\rho 2}^{\epsilon}} \frac{G_{\nu 2}'(\gamma_{\rho 2}^{\epsilon} a)}{G_{\nu 2}(\gamma_{\rho 2}^{\epsilon} a)} \right], \tag{15b}$$

where $\gamma = \alpha + \mathrm{j}\beta$ is the complex wave propagation constant in the axial direction of the waveguide, $\gamma_{\rho 1} = \sqrt{\gamma^2 + k_0^2}$, and $G_{\nu_{\mu}} = Y_{\nu_{\mu}}'(\gamma_{\rho 2}^{\mu} b) J_{\nu_{\mu}}'(\gamma_{\rho 2}^{\mu} \rho) - J_{\nu_{\mu}}'(\gamma_{\rho 2}^{\mu} b) Y_{\nu_{\mu}}'(\gamma_{\rho 2}^{\mu} \rho)$ is a combination of Bessel (J_ν) and Neumann (Y_ν) functions. The roots of (15a) and (15b) correspond to the EH mode and HE mode cutoff frequencies, respectively. Plotting the cutoff frequency with respect to liner permittivity for each mode leads to an interesting result for the HE_{11} mode: the cutoff frequency is strongly reduced for negative and near-zero values of permittivity. This mode shows weak, collimated fields in the centre region and strong fields in the liner. Consider a thin liner similar to the case studied in [79]. For an aperture with $b = 140$ nm and $a = 120$ nm, the cutoff frequency of the HE_{11} mode is plotted with respect to the anisotropic ϕ and ρ liner permittivity components in Figure 14(a). Clearly, for a thin liner, the ϕ component has very little effect on the frequency-reduced HE_{11} modal cutoff frequency.
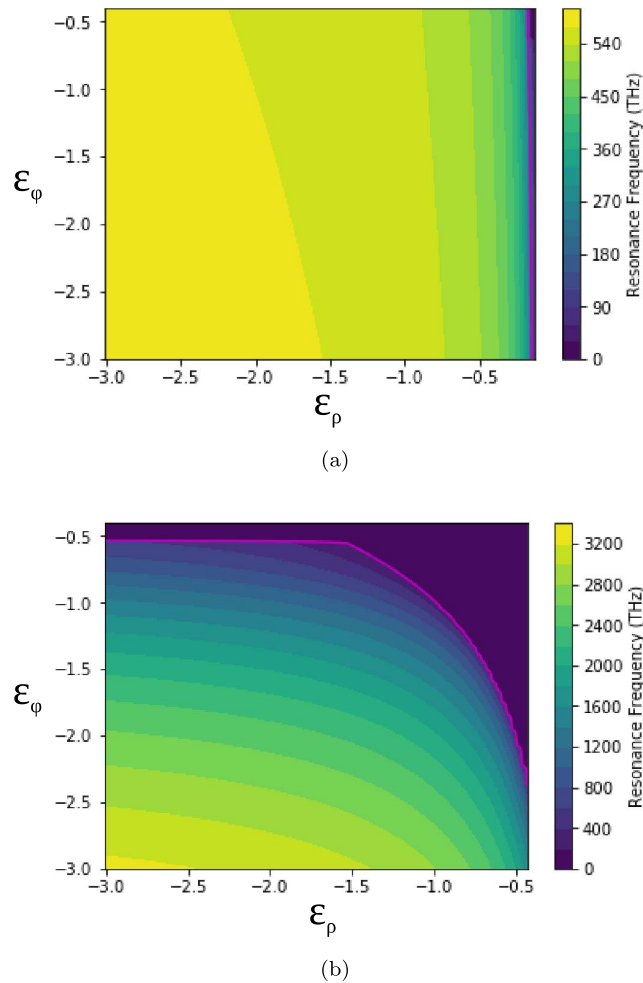
(a)

(b)

Figure 14. Surface plot of HE_{11} cutoff frequency with respect to anisotropic liner permittivity parameters for (a) a thin liner ($b = 140$ nm, $a = 120$ nm), and (b) a thick liner ($b = 140$ nm, $a = 14$ nm). The magenta line denotes 193 THz, or 1.55 μm, the wavelength of optical telecommunications.

If the inner radius is reduced to $a = 14$ nm, as plotted in Figure 14(b), the contribution from ϵ_ϕ is as important as the ϵ_ρ component given the higher filling factor of the aperture. As permittivity nears zero, the resonance frequency is reduced to the electrostatic condition (DC), as was observed for the metamaterial-lined PEC waveguide. Frequency-reduced resonance occurs for either ϵ_ρ or ϵ_ϕ, whereas the isotropic case required ϵ_ρ be near zero. A slice taken from the lower left to the top right of the plot extracts the response for an isotropic liner permittivity, and it can be seen that for a thick, isotropic liner, the resonance frequency saturates at DC for a much higher absolute value of permittivity (i.e. near $(-1, -1)$) than for either anisotropic parameter, and is thus more sensitive to very small changes in permittivity.

The interested reader may find more information on other 3D spherical and cylindrical core-shell structures that support compact resonances with arbitrary anisotropic permittivities and permeabilities in some of the following references: [13, 59, 79, 83–87].
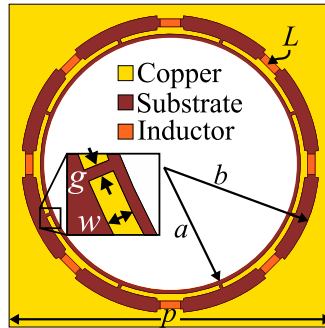
Figure 15. Practical implementation of the ENNZ-metamaterial lined aperture from [80], Figure 1(c). *a*, *b*, and *p* are borrowed from Figure 12. *L* refers to discrete radial inductors, *w* is the azimuthal trace width, and *g* is the azimuthal capacitive gap width. Reprinted with permission from [80] © The Optical Society.

5.2. *Microwave implementation*

The practical implementation of the ENNZ-lined aperture takes on a very similar geometry to the practical ENNZ-lined waveguide, but rather than a cascade of identical liner rings, includes only a single liner layer, as shown in Figure 15 [80]. If the liner (Figure 16(a)) is straightened out and viewed as an azimuthally directed CPS TL (Figure 16(b)), the well-known TL-metamaterial theory prescribes that a positive susceptance placed in shunt leads to a homogenized negative effective permittivity (Figure 16(c)) [43, 79]. The positive susceptance is created using shunt discrete inductors (*L*), and series capacitors are used to suppress any azimuthal resonances. Eight unit-cells are arranged around the azimuth to create an effective medium that is polarization insensitive.

Printed components may also be used, and offer many advantages. They are simpler to fabricate, can be made conformal, are easy to modify/tune, and can be more accurately modeled in simulation. The fabricated ENNZ-lined aperture shown in Figure 17(a) uses printed dual-arm spiral inductors and small gap capacitors. This structure was patterned with an LPKF ProtoMat S62 mechanical milling machine, which uses a digitally controlled mechanical routing bit to remove the copper cladding from a microwave substrate with up to 100 μm precision, as shown in Figure 17(b). The experimental results match full-wave electromagnetic simulations performed in Ansys HFSS. The resonance frequency of the aperture can be tuned in the same way the waveguide cutoff frequency is tuned: stronger inductive loading or larger aperture size reduce the resonance frequency, while weaker inductive loading or smaller apertures increase the resonance frequency.

Compact resonance may also be achieved in a similar manner on a solid metallic "patch" that is the dual of the aperture case. The ENNZ-liner becomes a coating with strong series capacitive loading instead of shunt inductive loading, which leads to an MNNZ response. This structure, however, has less in common with the equivalent waveguide as the patch may support longitudinal electric fields on the surface of the central disc, whereas the fields inside the core of the waveguide must be zero.

5.3. *Optical implementation*

ENNZ-metamaterial-lined apertures can be translated from the microwave to the optical domain, where inductors can no longer be made from coiled wires and copper no longer acts as
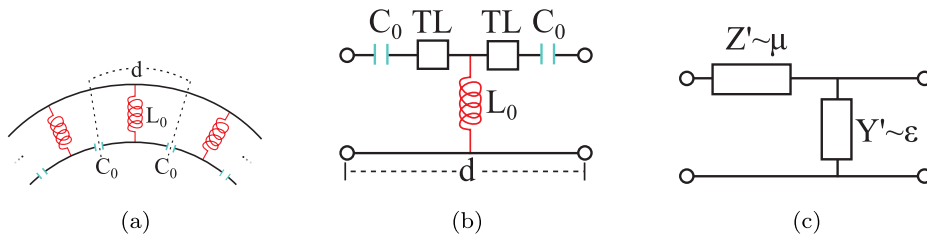
Figure 16. TL model for the ENNZ liner. (a) is the circuit equivalent of the liner with lumped components, (b) is the equivalent transmission-line model, and (c) is the homogenized TL-metamaterial model. © 2016 IEEE. Reprinted, with permission, from [79].
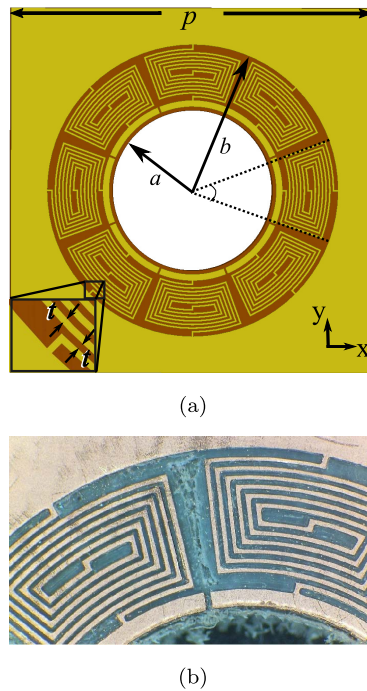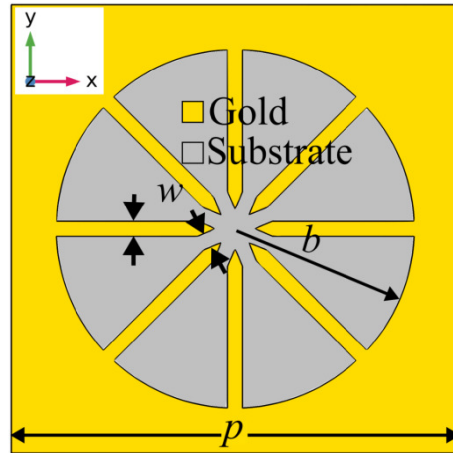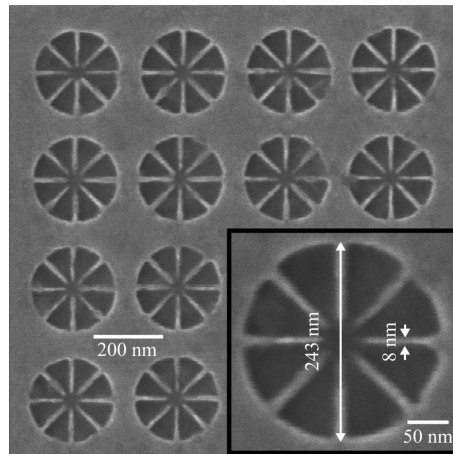

Figure 17. Printed ENNZ-metamaterial-lined aperture, (a) full aperture design, and (b) fabricated structure. © 2018 IEEE. Reprinted, with permission, from [88].

a perfect metal [89]. To implement an ENNZ liner, the concept of optical nanocircuits is invoked [90–94]. Optical nanocircuits generalize lumped circuit elements to apply not only to conduction currents (dominant at lower frequencies), but also to displacement currents (dominant at optical frequencies). Effectively, chains of nanoparticles with positive permittivity act as lumped optical capacitors, and nanoparticles with negative permittivity act as lumped optical inductors. It is well known that metals exhibit negative permittivity near and below their plasmonic resonance frequency, hence lumped inductors can be replaced with metallic nanoparticles, and lumped capacitors can be replaced with dielectric nanoparticles or air gaps. Notice that this is very similar to printed microwave components, however, the inductors no longer need to be meandered, hence an optical implementation of the ENNZ-lined aperture can be created by simply replacing the printed lumped inductors with nanowires.

(a)

(b)

Figure 18. Optical implementation of the thick-liner ENNZ-metamaterial-lined apertures: (a) designed structure, (b) fabricated structure using helium ion milling. © 2019 IEEE. Reprinted, with permission, from [89].

The properties of a printed inductor are much easier to control than those of a nanowire, thus a new mechanism was introduced to control the resonance frequency of the optical ENNZ-lined aperture: the liner thickness. As the size of the liner increases, the liner fields move further from the PEC boundary and may have both radial and azimuthal components. Hence the anisotropic model for the liner permittivity must be incorporated, as explained above. In fact, increasing the liner thickness allows a greater degree of miniaturization to be achieved than the isotropic liner for a given liner dispersion. The thickest possible liner extends nearly to the centre of the aperture, and is used for the optical implementation shown in Figure 18(a). This structure exhibits another interesting feature: the liner fields are strongly enhanced at the centre of the aperture. Plasmonic field enhancement of this nature is used to encourage low-probability scattering events such as Raman scattering, to increase sensor sensitivity, to encode information at a subwavelength scale, and more.

The structure was patterned into a 50 nm gold layer (which has low loss and is optically opaque) on a transparent glass substrate. A minimum feature size of 10 nm was chosen for maximum control over the nanowire plasmonic resonance frequency. Fabrication of such small features with large aspect ratios in metal films is an extreme challenge, and can only be accomplished by helium focused ion beam milling. The Zeiss Orion Nanofab Helium Ion Microscope was used to pattern the structure shown in Figure 18(b). Characterization efforts are ongoing.

Individually, metamaterial-loaded resonators can be used as subwavelength sensors in much the same way as the waveguides they are based on can be used as probes, however, because they are flat, another degree of freedom is available: 2D, flat arrays of subwavelength resonators, i.e., metasurfaces.

6. Periodic arrays (metasurfaces)

Expanding the scope of metamaterial-loaded resonators to 2D grids introduces a host of features not present for a single aperture or waveguide, some of which include: diffraction anomalies, interaperture coupling and excitation angles.

6.1. *Extraordinary optical transmission*

Recent interest in diffraction anomalies was sparked by Ebbesen's observation of extraordinary optical transmission (EOT) in 1998 [95]. Ebbesen *et al.* patterned a silver film with a square array of nanoholes and measured the optical transmission. They were surprised to find that when the period of the array was exactly one wavelength, near-perfect transmission was observed, counter to the classical Bethe theory of diffraction by subwavelength holes [81]. Although this was initially interpreted using concepts of surface plasmons, and later spoof surface plasmons, the current more rigorous understanding is on the basis of diffraction anomalies and the generation of a leaky-wave field that couples to the incoming and outgoing free-space modes [96–99]. Modern work on the subject consists of generalizing diffraction anomalies to new structures with cartesian, polar and spherical periodicity. Generally, diffraction anomalies occur for periodic structures with wavelength-scale spacings.

The current understanding of EOT clearly establishes that diffraction anomalies are not responsible for the increased transmission seen in arrays of metamaterial-lined apertures as the spacing between apertures/resonators is much too small.

6.2. *Inter-aperture coupling*

Another complication introduced by the arraying of apertures is the ability to couple apertures. This effect makes the design of arrays significantly more challenging, as individually designed elements may act very differently in combination. For electrically large elements, such as those used in frequency-selective surfaces (FSS), the coupling is generally low and the resonator's interaction can be well-modeled with antenna array theory or coupled-line theory [100,101]. In the case of closely spaced, electrically small elements (i.e. resonant metasurfaces), however, the energy stored by the resonator in the near-field will generally lead to strong coupling with adjacent elements [102,103]. The ENNZ-metamaterial-lined aperture avoids this issue by strongly confining the fields at resonance (plotted in Figure 19) to the liner area, which allows both uniform and nonuniform arrays to be designed from individual unit cells.
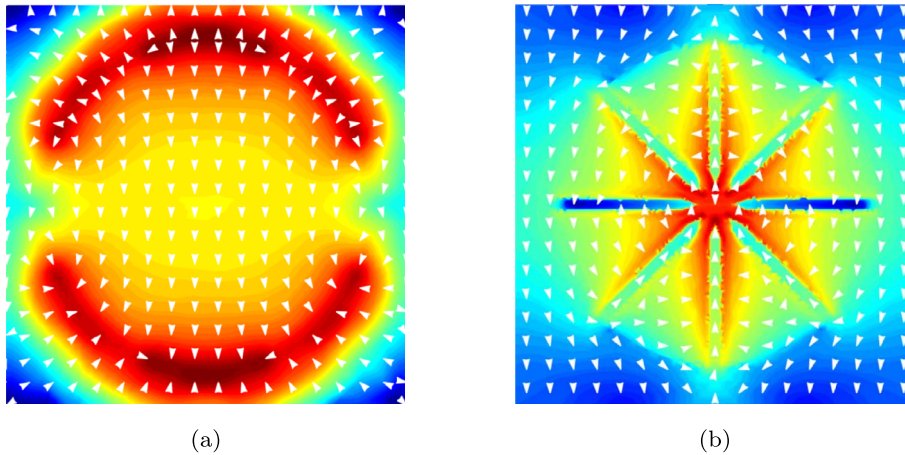
Figure 19. Complex electric-field magnitude and vector direction for (a) the microwave, thin-liner case, where fields are confined to the liner region, and (b) the optical, thick-liner case, where fields are confined to the centre of the aperture. © 2019 IEEE. Reprinted, with permission, from [89].

6.3. *Excitation polarization and angle*

Although complications exist for periodic arrays, there are also many advantages over waveguides. The in-plane periodicity makes fabrication much simpler than the multilayer fabrication required for waveguides. Rather than using different waveguide excitations, metasurfaces are studied under the effect of incident plane waves. These plane waves can be arbitrarily polarized and incident from any angle. TE and TM plane waves are degenerate for normal incidence, but lead to very different excitation conditions off-normal. For example, assuming no bianisotropy, the z-component (x–y periodicity) of the magnetic field for a TE polarized wave can excite a planar magnetic dipolar resonance, whereas the TM polarized wave cannot. Furthermore, off-normal incidence effectively changes the period of the metasurface with respect to the wavelength of the incoming wave. This emphasizes the need for extremely subwavelength and decoupled unit cells, as the effective periodicity variation changes the response less, and hence gives a stable response for wide angles of incidence.

The incident polarization that the ENNZ-metamaterial-lined aperture metasurface responds to may be controlled by changing the azimuthal periodicity. At first, 8 unit cells per azimuthal period was chosen in part to be polarization insensitive and better comparable to the waveguide case, but if only 2 unit cells are used, the resonance only occurs for one incident linear polarization. An array of polarization-sensitive apertures can be used as a polarization splitter or shield. The resonance is largely independent of elements placed on the opposing axis, and dual-band or dual-polarization metasurfaces with independently controllable bands can be made on a single layer.

Any fully planar MTS cannot produce a magnetic dipole resonance for normal incidence as a loop must be formed longitudinally in the current path. Unfortunately, imparting the full 2π transmission phase shift required for phase-gradient MTSs to an incoming plane wave requires the excitation of both a magnetic- and an electric-dipolar resonance, and normal incidence is often the most practical setup [104]. For this reason, many modern metasurface designers have moved towards multilayer systems. Recall that the practical implementation of the metamaterial-lined waveguide required essentially cascading metamaterial-lined apertures, hence the theory
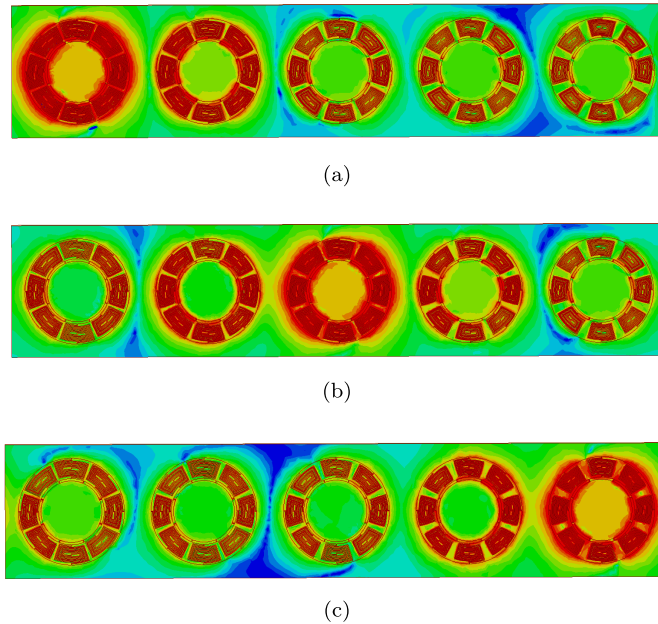
(a)

(b)

(c)

Figure 20. Complex electric-field magnitudes at successive resonance frequencies for a 5 × 1 nonuniform array of ENNZ-metamaterial-lined apertures. (a) 2.695 GHz. (b) 2.965 GHz. (c) 3.30 GHz. © 2018 IEEE. Reprinted, with permission, from [88].

lends well to creating multilayer metamaterial-lined aperture metasurfaces, but further study will be required to fully develop the required design procedures.

7. Applications

ENNZ-lined aperture metasurfaces share some applications with the equivalent waveguide. Sensing of dielectric materials may be done in both cases by passing liquids through the empty centre, where shifts in resonance or cutoff frequency can be associated with changes in permittivity. The metasurface, however, may improve this device due to its added ability to parallelize a process with many adjacent apertures under different sensing conditions at a subwavelength scale. For example, Baladi *et al.* showed that by creating a nonuniform array of 5 ENNZ-lined apertures with different inductors, obstacles can be detected in front of each aperture individually by examining the disappearance of each corresponding resonance in the transmitted spectrum, at a resolution better than $\lambda/6$ [88]. Figure 20 shows the electric-field magnitude at three of the resonance frequencies. It can clearly be seen that only one aperture reacts at each frequency.

In fact, the resonance frequency of an ENNZ-lined aperture is most sensitive to the permittivity of the liner, which may make an optical implementation where an analyte may also pass through the liner much more sensitive. The metasurface may be made tunable by the introduction of varactors or active elements, which can allow for flexibility in shielding, filtering, and sensing. Furthermore, introducing nonlinear optical materials into the optical ENNZ-metamaterial-lined apertures can allow for high-speed optical switching phenomena to occur. The strong field enhancement at the centre of the optical ENNZ-metamaterial-lined metasurface can be used to strongly excite optical nonlinearities for frequency conversion and its subwavelength nature could be used to increase the density of optical storage media.

8. Outlook

There are many future directions for metamaterial-liner-loaded metasurfaces. Immediate work on adapting the already proven structures to exhibit polarization sensitivity will open many options in polarizing and shielding devices, and exploring the response of the complementary metafilm structure will allow control over both reflection and transmission. Further, multilayer metasurfaces with robust design methods are very active, but will take some development to allow for non-uniform liners in the axial direction.

For the optical case, once the characterization problem is solved, polarization-sensitive structures will allow the resonance frequency to be shifted to the visible, where subwavelength apertures may cheaply increase the resolution of conventional photolithography or qualitatively sense analyte concentration in fluids by changing transmission colour.

The nanostructured fibers presented here, even though the structure is at a subwavelength size, will always create some scattering of light and will have high throughput losses. Hence it is never envisaged that metamaterial filled waveguides will be utilized for long distance propagation, for example, in optical communications. Instead, these waveguides possess unique properties that make them suitable for other applications. For example, end-coupling or butt-coupling of the fiber to the near-field modes of a source has been shown to be easily possible for these anisotropic or hyperbolic fibers. These have potential applications as high throughput probes for near-field optical microscopy. Further, as the fields of the higher-order modes tend to spread out throughout the cross-section of the optical fiber, there are distinct advantages against spatial hole-burning and bleaching processes due to large localized fields. Such processes may provide support for applications such as laser amplification, parametric amplification, harmonic generation, or self-phase modulation that can occur over short lengths of the waveguide.

In another manifestation, where the central core region is empty or filled with a dielectric material and the cladding consists of an anisotropic metamaterial, modes concentrated near the centre may be effectively coupled to other materials placed in the central core region. Behaviour of emitting molecules in such regions will be drastically affected due to the large field enhancements as well as the modified density of modes available. Such optical fibers may also be effectively controlled by microfluidic flows in the central core region of the optical fibers. The hollow-core waveguide may be utilized for sensing applications, where a solution is pumped through the central core and the molecules or bacteria, if present, will scatter the light in fiber and modify the transmittance to enable their sensing.

The nanoporous-alumina-based fibers make available an immensely large porous volume which may be utilized for adsorption processes. The presence of adsorbed molecules on the optical fiber will result in an effective refractive index change of the optical fiber and selectively change the transmission or reflection of certain modes of the optical fiber, making them good candidates for sensor purposes. Incorporation of any other media, such as a liquid or a polymer in the nanopores of the optical fiber may be easily carried out by immersing of a portion of the optical fiber in the liquid or the polymer melt. Due to capillary action, the liquid or the polymer would be strongly drawn into the nanopores of the optical fiber. Embedding laser amplifying media, such as laser dyes, into the nanopores of the alumina microtubes would make them potential candidates for fiber amplifiers.

Further, it should be noted that deeply subwavelength and decoupled unit cells are a necessity here for the effective medium approximation to hold, particularly for waves with large transverse wave-vectors such as those that occur at large oblique angles of incidence or become evanescent in the waveguide. Having highly subwavelength structure to form the metamaterial is also very beneficial to reduce the scattering and wave-guide losses. This is very important for large trans-

verse order waveguide modes in the indefinite permittivity/permeability waveguides, where the fields rapidly vary along the angular or transverse directions in the interior of the waveguide.

We conclude by noting that in almost all reports on this topic, the axes of the anisotropic medium and the waveguide coincide, while the metamaterial axes could be arbitrarily oriented. The very large parameter space made available for exploration by anisotropic and hyperboic metamaterials in the context of waveguides makes it certain that many important new phenomena and applications await us in the future.

Acknowledgements

References

[1] J. B. Pendry, A. Holden, W. Stewart, I. Youngs, "Extremely low frequency plasmons in metallic mesostructures", *Phys. Rev. Lett.* **76** (1996), no. 25, article no. 4773.

[2] J. B. Pendry, A. J. Holden, D. J. Robbins, W. Stewart *et al.*, "Magnetism from conductors and enhanced nonlinear phenomena", *IEEE Trans. Microw. Theory Tech.* **47** (1999), no. 11, p. 2075-2084.

[3] V. G. Veselago, "The electrodynamics of substances with simultaneously negative values of ϵ and μ", *Phys.-Usp.* **10** (1968), no. 4, p. 509-514.

[4] D. R. Smith, W. J. Padilla, D. Vier, S. C. Nemat-Nasser, S. Schultz, "Composite medium with simultaneously negative permeability and permittivity", *Phys. Rev. Lett.* **84** (2000), no. 18, article no. 4184.

[5] J. B. Pendry, "Negative refraction makes a perfect lens", *Phys. Rev. Lett.* **85** (2000), no. 18, article no. 3966.

[6] N. M. Litchinitser, A. I. Maimistov, I. R. Gabitov, R. Z. Sagdeev, V. M. Shalaev, "Metamaterials: electromagnetic enhancement at zero-index transition", *Opt. Lett.* **33** (2008), no. 20, p. 2350-2352.

[7] S. Zhang, W. Fan, N. Panoiu, K. Malloy, R. Osgood, S. Brueck, "Experimental demonstration of near-infrared negative-index metamaterials", *Phys. Rev. Lett.* **95** (2005), no. 13, article no. 137404.

[8] D. Smith, D. Vier, T. Koschny, C. Soukoulis, "Electromagnetic parameter retrieval from inhomogeneous metamaterials", *Phys. Rev. E* **71** (2005), no. 3, article no. 036617.

[9] D. Smith, D. Schurig, "Electromagnetic wave propagation in media with indefinite permittivity and permeability tensors", *Phys. Rev. Lett.* **90** (2003), no. 7, article no. 077405.

[10] Z. Jacob, L. V. Alekseyev, E. Narimanov, "Optical hyperlens: far-field imaging beyond the diffraction limit", *Opt. Express* **14** (2006), no. 18, p. 8247-8256.

[11] H. N. Krishnamoorthy, Z. Jacob, E. Narimanov, I. Kretzschmar, V. M. Menon, "Topological transitions in metamaterials", *Science* **336** (2012), no. 6078, p. 205-209.

[12] Q. Zhang, T. Jiang, Y. Feng, "Slow-light propagation in a cylindrical dielectric waveguide with metamaterial cladding", *J. Phys. D: Appl. Phys.* **44** (2011), no. 47, article no. 475103.

[13] D. Pratap, S. A. Ramakrishna, J. G. Pollock, A. K. Iyer, "Anisotropic metamaterial optical fibers", *Opt. Express* **23** (2015), no. 7, article no. 9074.

[14] S. Atakaramians, A. Argyros, S. C. Fleming, B. T. Kuhlmey, "Hollow-core waveguides with uniaxial metamaterial cladding: modal equations and guidance conditions", *J. Opt. Soc. Am. B* **29** (2012), no. 9, p. 2462-2477.

[15] A. Alù, N. Engheta, "Guided modes in a waveguide filled with a pair of single-negative (sng), double-negative (dng), and/or double-positive (dps) layers", *IEEE Trans. Microw. Theory Tech.* **52** (2004), no. 1, p. 199-210.

[16] A. Bhardwaj, K. V. Srivastava, S. A. Ramakrishna, "Enhanced coupling of light from subwavelength sources into a hyperbolic metamaterial fiber", *J. Lightwave Technol.* **37** (2019), no. 13, p. 3064-3072.

[17] J. G. Pollock, A. K. Iyer, "Below-cutoff propagation in metamaterial-lined circular waveguides", *IEEE Trans. Microw. Theory Tech.* **61** (2013), no. 9, p. 3169-3178.

[18] I. V. Shadrivov, A. A. Sukhorukov, Y. S. Kivshar, "Guided modes in negative-refractive-index waveguides", *Phys. Rev. E* **67** (2003), no. 5, article no. 057602.

[19] A. Bhardwaj, K. V. Srivastava, S. A. Ramakrishna, "Propagation of wave in a cylindrical waveguide filled with hyperbolic negative index medium", *Microw. Opt. Technol. Lett.* **62** (2020), no. 11, p. 3385-3390.

[20] K. Porsezian, V. C. Kuriakose, *Optical Solitons: Theoretical and Experimental Challenges, Vol. 613*, Springer Science & Business Media, Heidelberg, Germany, 2003.

[21] P. Russell, "Photonic crystal fibers", *Science* **299** (2003), no. 5605, p. 358-362.

[22] N. Singh, A. Tuniz, R. Lwin, S. Atakaramians, A. Argyros, S. C. Fleming, B. T. Kuhlmey, "Fiber-drawn double split ring resonators in the terahertz range", *Opt. Mater. Express* **2** (2012), no. 9, p. 1254-1259.

[23] M. G. Silveirinha, C. A. Fernandes, "Nonresonant structured material with extreme effective parameters", *Phys. Rev. B* **78** (2008), no. 3, article no. 033108.

[24] C. R. Simovski, P. A. Belov, A. V. Atrashchenko, Y. S. Kivshar, "Wire metamaterials: physics and applications", *Adv. Mater.* **24** (2012), no. 31, p. 4229-4248.

[25] M. Kadic, S. Guenneau, S. Enoch, S. A. Ramakrishna, "Plasmonic space folding: focusing surface plasmons via negative refraction in complementary media", *ACS Nano* **5** (2011), no. 9, p. 6819-6825.

[26] S. A. Ramakrishna, T. M. Grzegorczyk, *Physics and Applications of Negative Refractive Index Materials*, CRC Press, Bellingham, Washington, USA, 2008.

[27] J. B. Pendry, A. Holden, D. Robbins, W. Stewart, "Low frequency plasmons in thin-wire structures", *J. Phys.: Condens. Matter* **10** (1998), no. 22, article no. 4785.

[28] D. J. Bergman, "The dielectric constant of a composite material—a problem in classical physics", *Phys. Rep.* **43** (1978), no. 9, p. 377-407.

[29] T. G. Mackay, A. Lakhtakia, "Bruggeman formalism versus", *J. Nanophoton.* **6** (2012), no. 1, article no. 069501.

[30] S. Guenneau, F. Zolla, A. Nicolet, "Homogenization of 3d finite photonic crystals with heterogeneous permittivity and permeability", *Waves Random Complex Media* **17** (2007), no. 4, p. 653-697.

[31] A. Castanié, J.-F. Mercier, S. Félix, A. Maurel, "Generalized method for retrieving effective parameters of anisotropic metamaterials", *Opt. Express* **22** (2014), no. 24, p. 29937-29953.

[32] W. S. Weiglhofer, A. Lakhtakia, "On electromagnetic waves in biaxial bianisotropic media", *Electromagnetics* **19** (1999), no. 4, p. 351-362.

[33] X. Chen, B.-I. Wu, J. A. Kong, T. M. Grzegorczyk, "Retrieval of the effective constitutive parameters of bianisotropic metamaterials", *Phys. Rev. E* **71** (2005), no. 4, article no. 046610.

[34] C. E. Kriegler, M. S. Rill, S. Linden, M. Wegener, "Bianisotropic photonic metamaterials", *IEEE J. Sel. Top. Quantum Electron.* **16** (2009), no. 2, p. 367-375.

[35] T. G. Mackay, A. Lakhtakia, *Electromagnetic Anisotropy and Bianisotropy: A Field Guide*, World Scientific, Singapore, 2010.

[36] B. Gralak, M. Lequime, M. Zerrad, C. Amra, "Phase retrieval of reflection and transmission coefficients from Kramers–Kronig relations", *J. Opt. Soc. Am. A* **32** (2015), no. 3 (ts), p. 456-462.

[37] Y. Liu, S. Guenneau, B. Gralak, "Causality and passivity properties of effective parameters of electromagnetic multilayered structures", *Phys. Rev. B* **88** (2013), article no. 165104.

[38] A. Serdiukov, I. Semchenko, S. Tertyakov, A. Sihvola, *Electromagnetics of Bi-anisotropic Materials-Theory and Application, Vol. 11*, Gordon and Breach Science Publishers, Norwich, UK, 2001.

[39] G. Sauer, G. Brehm, S. Schneider, K. Nielsch, R. Wehrspohn, J. Choi, H. Hofmeister, U. Gösele, "Highly ordered monocrystalline silver nanowire arrays", *J. Appl. Phys.* **91** (2002), no. 5, p. 3243-3247.

[40] R. Kumar, F. A. Inam, A. Ly, C. Bradac, S. A. Ramakrishna, "Silver columnar thin-film-based half-wavelength antennas for bright directional emission from nanodiamond nitrogen-vacancy centers", *Phys. Rev. Appl.* **11** (2019), no. 3, article no. 034002.

[41] A. Poddubny, I. Iorsh, P. Belov, Y. Kivshar, "Hyperbolic metamaterials", *Nat. Photon.* **7** (2013), no. 12, article no. 948.

[42] L. Ferrari, C. Wu, D. Lepage, X. Zhang, Z. Liu, "Hyperbolic metamaterials and their applications", *Prog. Quantum Electron.* **40** (2015), p. 1-40.

[43] G. V. Eleftheriades, A. K. Iyer, P. C. Kremer, "Planar negative refractive index media using periodically LC loaded transmission lines", *IEEE Trans. Microw. Theory Tech.* **50** (2002), no. 12, p. 2702-2712.

[44] C. Caloz, T. Itoh, "Novel microwave devices and structures based on the transmission line approach of meta-materials", in *IEEE MTT-S International Microwave Symposium Digest, 2003*, vol. 1, IEEE, 2003, p. 195-198.

[45] A. Lai, C. Caloz, T. Itoh, "Transmission line based metamaterials and their microwave applications", *Microw. Mag.* **5** (2004), no. 3, p. 34-50.

[46] I. Nefedov, S. Tretyakov, "Waveguide containing a backward-wave slab", *Radio Sci.* **38** (2003), no. 6, p. 9-1.

[47] A. Alù, N. Engheta, "Pairing an epsilon-negative slab with a mu-negative slab: resonance, tunneling and trans-parency", *IEEE Trans. Antennas Propag.* **51** (2003), no. 10, p. 2558-2571.

[48] Y. Satomura, M. Matsuhara, N. Kumagai, "Analysis of electromagnetic-wave modes in anisotropic slab waveguide", *IEEE Trans. Microw. Theory Tech.* **22** (1974), no. 2, p. 86-92.

[49] I. V. Lindell, S. Ilvonen, "Waves in a slab of uniaxial bw medium", *J. Electromagn. Waves Appl.* **16** (2002), no. 3, p. 303-318.

[50] B.-I. Wu, T. M. Grzegorczyk, Y. Zhang, J. A. Kong, "Guided modes with imaginary transverse wave number in a slab waveguide with negative permittivity and permeability", *J. Appl. Phys.* **93** (2003), no. 11, p. 9386-9388.

[51] Y. Xu, "A study of waveguides filled with anisotropic metamaterials", *Microw. Opt. Technol. Lett.* **41** (2004), no. 5, p. 426-431.

[52] S. Hrabar, J. Bartolic, Z. Sipus, "Waveguide miniaturization using uniaxial negative permeability metamaterial", *IEEE Trans. Antennas Propag.* **53** (2005), no. 1, p. 110-119.

[53] R. Marques, J. Martel, F. Mesa, F. Medina, "Left-handed-media simulation and transmission of EM waves in sub-wavelength split-ring-resonator-loaded metallic waveguides", *Phys. Rev. Lett.* **89** (2002), no. 18, article no. 183901.

[54] R. Yang, Y. Xie, X. Yang, R. Wang, B. Chen, "Fundamental modal properties of srr metamaterials and metamaterial based waveguiding structures", *Opt. Express* **17** (2009), no. 8, p. 6101-6117.

[55] F.-Y. Meng, J.-H. Fu, G.-H. Yang, Q. Wu, L.-W. Li, "Backward and forward waves in a uniaxial anisotropic metamaterial waveguide", in *2008 International Conference on Microwave and Millimeter Wave Technology*, vol. 1, IEEE, 2008, p. 54-57.

[56] H. Zhu, X. Yin, L. Chen, Z. Zhu, X. Li, "Manipulating light polarizations with a hyperbolic metamaterial waveguide", *Opt. Lett.* **40** (2015), no. 20, p. 4595-4598.

[57] D. J. Roth, A. V. Krasavin, A. Wade, W. Dickson, A. Murphy, S. Kéna-Cohen, R. Pollard, G. A. Wurtz, D. Richards, S. A. Maier *et al.*, "Spontaneous emission inside a hyperbolic metamaterial waveguide", *ACS Photon.* **4** (2017), no. 10, p. 2513-2521.

[58] H. Ruan, Y. Shuang, L. Li, T. Cui, "Extraordinary optical transmission through a rectangular hole filled with extreme uniaxial metamaterials", *Opt. Lett.* **42** (2017), no. 12, p. 2386-2389.

[59] J. G. Pollock, A. K. Iyer, D. Pratap, S. A. Ramakrishna, "A class of circular waveguiding structures containing cylindrically anisotropic metamaterials: Applications from radio frequency/microwave to optical frequencies", *J. Appl. Phys.* **119** (2016), no. 8, article no. 083103.

[60] T. Dunster, "Bessel functions of purely imaginary order, with an application to second-order linear differential equations having a large parameter", *SIAM J. Math. Anal.* **21** (1990), no. 4, p. 995-1018.

[61] C. Chapman, "The asymptotic theory of dispersion relations containing Bessel functions of imaginary order", *Proc. R. Soc. A* **468** (2012), no. 2148, p. 4008-4023.

[62] A. Tuniz, B. Kuhlmey, R. Lwin, A. Wang, J. Anthony, R. Leonhardt, S. Fleming, "Drawn metamaterials with plasmonic response at terahertz frequencies", *Appl. Phys. Lett.* **96** (2010), no. 19, article no. 191101.

[63] A. Tuniz, R. Lwin, A. Argyros, S. C. Fleming, B. T. Kuhlmey, "Fabricating metamaterials using the fiber drawing method", *J. Vis. Exp.* **68** (2012), article no. e4299.

[64] A. Tuniz, K. J. Kaltenecker, B. M. Fischer, M. Walther, S. C. Fleming, A. Argyros, B. T. Kuhlmey, "Metamaterial fibres for subdiffraction imaging and focusing at terahertz frequencies over optically long distances", *Nat. Commun.* **4** (2013), article no. 2706.

[65] M. Yan, N. A. Mortensen, "Hollow-core infrared fiber incorporating metal-wire metamaterial", *Opt. Express* **17** (2009), no. 17, p. 14851-14864.

[66] D. Pratap, A. Bhardwaj, S. A. Ramakrishna, "Inhomogeneously filled, cylindrically anisotropic metamaterial optical fiber", *J. Nanophoton.* **12** (2018), no. 3, article no. 033002.

[67] D. Pratap, S. A. Ramakrishna, Nanoporous alumina microtubes for metamaterial and plasmonic applications, *preprint*, arXiv:1903.10296 (2018).

[68] W. Cai, V. Shalaev, *Optical Metamaterials: Fundamentals and Applications*, Springer, New York, 2009.

[69] M. J. Weber, *Handbook of Optical Materials*, CRC Press, Washington, D.C., 2003.

[70] C.-C. Lai, C.-Y. Lo, J.-Z. Huang, C.-C. F. Chiang, D. H. Nguyen, Y.-P. Chen, C.-D. Liao, "Architecting a nonlinear hybrid crystal–glass metamaterial fiber for all-optical photonic integration", *J. Mater. Chem. C* **6** (2018), no. 7, p. 1659-1669.

[71] C.-C. Lai, C.-Y. Lo, T.-H. Hsieh, W.-S. Tsai, D. H. Nguyen, Y.-R. Ma, "Ligand-driven and full-color-tunable fiber source: toward next-generation clinic fiber-endoscope tomography with cellular resolution", *ACS Omega* **1** (2016), no. 4, p. 552-565.

[72] C.-C. Lai, C.-Y. Lo, D. H. Nguyen, J.-Z. Huang, W.-S. Tsai, Y.-R. Ma, "Atomically smooth hybrid crystalline-core glass-clad fibers for low-loss broadband wave guiding", *Opt. Express* **24** (2016), no. 18, p. 20089-20106.

[73] A. Bhardwaj, K. V. Srivastava, S. A. Ramakrishna, "Hyperbolic metamaterial near-field coupler", in *2019 IEEE Asia-Pacific Microwave Conference (APMC)*, IEEE, 2019, p. 1736-1738.

[74] J. G. Pollock, A. K. Iyer, "Miniaturized circular-waveguide probe antennas using metamaterial liners", *IEEE Trans. Antennas Propag.* **63** (2014), no. 1, p. 428-433.

[75] J. G. Pollock, A. K. Iyer, "Effective-medium properties of cylindrical transmission-line metamaterials", *IEEE Antennas Wirel. Propag. Lett.* **10** (2011), p. 1491-1494.

[76] P. K. Choudhury, W. K. Soon, "On the tapered optical fibers with radially anisotropic liquid crystal clad", *Prog. Electromagn. Res.* **115** (2011), p. 461-475.

[77] M. M. Hasan, D. S. Kumar, M. R. C. Mahdy, D. N. Hasan, M. A. Matin, "Robust optical fiber using single negative metamaterial cladding", *IEEE Photon. Technol. Lett.* **25** (2013), no. 11, p. 1043-1046.

[78] S. Hou, S. Zhang, Y. Liu, D. Wang, J. Lei, "Investigation on characteristics of w-type fiber with an inner cladding made of negative refractive index materials", *Optik* **125** (2014), no. 20, p. 6127-6130.

[79] J. G. Pollock, A. K. Iyer, "Experimental verification of below-cutoff propagation in miniaturized circular waveguides using anisotropic ENNZ metamaterial liners", *IEEE Trans. Microw. Theory Tech.* **64** (2016), no. 4, p. 1297-1305.

[80] E. Baladi, J. G. Pollock, A. K. Iyer, "New approach for extraordinary transmission through an array of subwavelength apertures using thin ENNZ metamaterial liners", *Opt. Express* **23** (2015), no. 16, article no. 20356.

[81] H. A. Bethe, "Theory of diffraction by small holes", *Phys. Rev.* **66** (1944), p. 163-182.

[82] M. F. Limonov, M. V. Rybin, A. N. Poddubny, Y. S. Kivshar, "Fano resonances in photonics", *Nat. Photon.* **11** (2017), no. 9, p. 543-554.

[83] R. W. Ziolkowski, A. Erentok, "Metamaterial-based efficient electrically small antennas", *IEEE Trans. Antennas Propag.* **54** (2006), no. 7, p. 2113-2130.

[84] A. Alù, N. Engheta, "Polarizabilities and effective parameters for collections of spherical nanoparticles formed by pairs of concentric double-negative, single-negative, and/or double-positive metamaterial layers", *J. Appl. Phys.* **97** (2005), no. 9, article no. 094310.

[85] N. Engheta, "An idea for thin subwavelength cavity resonators using metamaterials with negative permittivity and permeability", *IEEE Antennas Wirel. Propag. Lett.* **1** (2002), p. 10-13.

[86] A. Alù, N. Engheta, "An overview of salient properties of planar guided-wave structures with Double-Negative (DNG) and Single-Negative (SNG) layers", in *Negative-Refraction Metamaterials*, John Wiley & Sons, Inc., Hoboken, NJ, USA, 2005, p. 339-380.

[87] A. Alu, N. Engheta, "Guided modes in a waveguide filled with a pair of Single-Negative (SNG), Double-Negative (DNG), and/or Double-Positive (DPS) layers", *IEEE Trans. Microw. Theory Tech.* **52** (2004), no. 1, p. 199-210.

[88] E. Baladi, A. K. Iyer, "Far-field magnification of subdiffraction conducting features using metamaterial-lined aperture arrays", *IEEE Trans. Antennas Propag.* **66** (2018), no. 7, p. 3482-3490.

[89] M. Semple, E. Baladi, A. K. Iyer, "Optical metasurface based on subwavelength nanoplasmonic metamaterial-lined apertures", *IEEE J. Sel. Top. Quantum Electron.* **25** (2019), no. 3, p. 1-8.

[90] A. Alu, N. Engheta, "Optical metamaterials based on optical nanocircuits", *Proc. IEEE* **99** (2011), no. 10, p. 1669-1681.

[91] N. Engheta, "From RF circuits to optical nanocircuits", *IEEE Microw. Mag.* **13** (2012), no. 4, p. 100-113.

[92] M. G. Silveirinha, A. Alù, J. Li, N. Engheta, "Nanoinsulators and nanoconnectors for optical nanocircuits", *J. Appl. Phys.* **103** (2008), no. 6, article no. 064305.

[93] H. Caglayan, S.-H. Hong, B. Edwards, C. R. Kagan, N. Engheta, "Near-infrared metatronic nanocircuits by design", *Phys. Rev. Lett.* **111** (2013), no. 7, article no. 073904.

[94] N. Engheta, "Circuits with light at nanoscales: optical nanocircuits inspired by metamaterials", *Science (New York, N.Y.)* **317** (2007), no. 5845, p. 1698-1702.

[95] T. W. Ebbesen, H. J. Lezec, H. F. Ghaemi, T. Thio, P. A. Wolff, "Extraordinary optical transmission through sub-wavelength hole arrays", *Nature* **391** (1998), no. 6668, p. 667-669.

[96] J. B. Pendry, L. Martín-Moreno, F. J. Garcia-Vidal, "Mimicking surface plasmons with structured surfaces", *Science (New York, N.Y.)* **305** (2004), no. 5685, p. 847-848.

[97] R. W. Wood, "On a remarkable case of uneven distribution of light in a diffraction grating spectrum", *Proc. Phys. Soc. Lond.* **18** (1902), no. 1, p. 269.

[98] A. Hessel, A. A. Oliner, "A new theory of wood's anomalies on optical gratings", *Appl. Opt.* **4** (1965), no. 10, p. 1275-1297.

[99] F. Medina, F. Mesa, R. Marques, "Extraordinary transmission through arrays of electrically small holes from a circuit theory perspective", *IEEE Trans. Microw. Theory Tech.* **56** (2008), no. 12, p. 3108-3120.

[100] S. Ghosh, K. V. Srivastava, "An equivalent circuit model of FSS-based metamaterial absorber using coupled line theory", *IEEE Antennas Wirel. Propag. Lett.* **14** (2015), p. 511-514.

[101] B. B. A. Munk, *Frequency Selective Surfaces: Theory and Design*, John Wiley & Sons, New York, USA, 2000.

[102] N. Liu, H. Liu, S. Zhu, H. Giessen, "Stereometamaterials", *Nat. Photon.* **3** (2009), no. 3, p. 157-162.

[103] M. Decker, R. Zhao, C. M. Soukoulis, S. Linden, M. Wegener, "Twisted split-ring-resonator photonic metamaterial with huge optical activity", *Opt. Lett.* **35** (2010), no. 10, article no. 1593.

[104] A. Arbabi, A. Faraon, "Fundamental limits of ultrathin metasurfaces", *Sci. Rep.* **7** (2017), no. 1, article no. 43722.